stricted specificity for squamous cell carcinoma of the head and neck. Cancer Res 1993;15;53:1461-8.
11. Hiratsuka H, Imamura M, Ishii Y, Kohama G, Kikuchi K. Immunohistologic detection of lymphocyte subpopulations infiltrating in human oral cancer with special reference to its clinical significance. Cancer 1984;1;53:2456-66.
12. Marincola FM, Jaffee EM, Hicklin DJ, Ferrone S. Escape of human solid tumors from T-cell recognition: molecular mechanisms and functional significance. Adv Immunol 2000;74:181-273.
13. Khong HT, Restifo NP. Natural selection of tumor variants in the generation of "tumor escape" phenotypes. Nat Immunol 2002;3:999-1005.
14. Ehrich EW, Devaux B, Rock EP, Jorgensen JL, Davis MM, Chien YH. T Cell receptor interaction with peptide/major histocompatibility complex (MHC) and superantigen/MHC ligands is dominated by antigen. J Exp Med 1993;1;178:713-22.
15. Matsutani T, Yoshioka T, Tsuruta Y, Iwagami S, Suzuki R. Analysis of TCRAV and TCRBV repertoires in healthy individuals by microplate hybridization assay. Hum Immunol 1997;56:57-69.
16. Engel I, Hedrick SM. Site-directed mutations in the VDJ junctional region of a T cell receptor beta chain cause changes in antigenic peptide recognition. Cell 1988 Aug 12;54:473-84.
17. Davis MM, Bjorkman PJ. T-Cell antigen receptor genes and T-cell recognition. Nature 1988;4;334:395-402.
18. Puisieux I, Even J, Pannetier C, Jotereau F, Favrot M, Kourilsky P. Oligoclonality of tumor-infiltrating lymphocytes from human melanomas. J Immunol 1994;15;153:2807-18.
19. Caignard A, Dietrich PY, Morand V, Lim A, Pannetier C, Leridant AM, et al. Evidence for T-cell clonal expansion in a patient with squamous cell carcinoma of the head and neck. Cancer Res 1994;1;54:1292-7.
20. Matsutani T, Shiiba K, Yoshioka T, Tsuruta Y, Suzuki R, Ochi T, et al. Evidence for existence of oligoclonal tumor-infiltrating lymphocytes and predominant production of T helper 1/T cytotoxic 1 type cytokines in gastric and colorectal tumors. Int J Oncol 2004;25:133-41.
21. Abbas AK, Murphy KM, Sher A. Functional diversity of helper T lymphocytes. Nature 1996;31;383:787-93.
22. Cerwenka A, Carter LL, Reome JB, Swain SL, Dutton RW. In vivo persistence of CD8 polarized T cell subsets producing type 1 or type 2 cytokines. J Immunol 1998;1;161:97-105.
23. Arden B, Clark SP, Kabelitz D, Mak TW. Human T-cell receptor variable gene segment families. Immunogenetics 1995;42:455-500.
24. Wei S, Charmley P, Robinson MA, Concannon P. The extent of the human germline T-cell receptor V beta gene segment repertoire. Immunogenetics 1994;40:27-36.
25. Koop BF, Rowen L, Wang K, Kuo CL, Seto D, Lenstra JA, et al. The human T-cell receptor TCRAC/TCRDC (C alpha/C delta) region: organization, sequence, and evolution of 97.6 kb of DNA. Genomics 1994;19:478-93.
26. Toyonaga B, Yoshikai Y, Vadasz V, Chin B, Mak TW. Organization and sequences of the diversity, joining, and constant region genes of the human T-cell receptor beta chain. Proc Natl Acad Sci U S A 1985;82:8624-8.
27. Girardi M, Oppenheim DE, Steele CR, Lewis JM, Glusac E, Filler R, et al. Regulation of cutaneous malignancy by gammadelta T cells. Science 2001;294(5542):605-9.
28. Gatti RA, Good RA. Occurrence of malignancy in immunodeficiency diseases. A literature review. Cancer 1971;28:89-98.
29. Naito Y, Saito K, Shiiba K, Ohuchi A, Saigenji K, Nagura H, et al. CD8+ T cells infiltrated within cancer cell nests as a prognostic factor in human colorectal cancer. Cancer Res 1998;15;58:3491-4.
30. Khuri FR, Shin DM, Glisson BS, Lippman SM, Hong WK. Treatment of patients with recurrent or metastatic squamous cell carcinoma of the head and neck: current status and future directions. Semin Oncol 2000;27:25-33.
31. Stoeckli SJ, Pfaltz M, Steinert H, Schmid S. Histopathological features of occult metastasis detected by sentinel lymph node biopsy in oral and oropharyngeal squamous cell carcinoma. Laryngoscope 2002;112:111-5.
32. Ferlito A, Shaha AR, Rinaldo A. The incidence of lymph node micrometastases in patients pathologically staged N0 in cancer of oral cavity and oropharynx. Oral Oncol 2002;38:3-5.

Reprint requests:

Yoshiki Hamada, DDS, PhD
Department of Oral and Maxillofacial Surgery
School of Dental Medicine
Tsurumi University
2-1-3 Tsurumi Tsurumi-ku
Yokohama, 230-8501
Japan
hamada-y@tsurumi-u.ac.jp

Biochemical and Biophysical Research Communications 409 (2011) 46–51

Contents lists available at ScienceDirect

Biochemical and Biophysical Research Communications

journal homepage: www.elsevier.com/locate/ybbrc

The ECS(SPSB) E3 ubiquitin ligase is the master regulator of the lifetime of inducible nitric-oxide synthase

Kazuma Matsumoto [a], Tadashi Nishiya [a,*], Satoshi Maekawa [a], Takahiro Horinouchi [a], Kouetsu Ogasawara [b], Takashi Uehara [c], Soichi Miwa [a]

[a] Department of Cellular Pharmacology, Hokkaido University Graduate School of Medicine, Sapporo 060-8638, Japan
[b] Department of Immunology, Institute of Development, Aging and Cancer (IDAC), Tohoku University, Sendai 980-8575, Japan
[c] Department of Medicinal Pharmacology, Graduate School of Medicine, Dentistry and Pharmaceutical Sciences, Okayama University, Okayama 700-8530, Japan

ARTICLE INFO

Article history:
Received 19 April 2011
Available online 28 April 2011

Keywords:
iNOS
ECS(SPSB)
CHIP
Ubiquitination
Proteasomal degradation

ABSTRACT

The ubiquitin–proteasome pathway is an important regulatory system for the lifetime of inducible nitric-oxide synthase (iNOS), a high-output isoform compared to neuronal NOS (nNOS) and endothelial NOS (eNOS), to prevent overproduction of NO that could trigger detrimental effects such as cytotoxicity. Two E3 ubiquitin ligases, Elongin B/C–Cullin-5–SPRY domain- and SOCS box-containing protein [ECS(SPSB)] and the C-terminus of Hsp70–interacting protein (CHIP), recently have been reported to target iNOS for proteasomal degradation. However, the significance of each E3 ubiquitin ligase for the proteasomal degradation of iNOS remains to be determined. Here, we show that ECS(SPSB) specifically interacted with iNOS, but not nNOS and eNOS, and induced the subcellular redistribution of iNOS from dense regions to diffused expression as well as the ubiquitination and proteasomal degradation of iNOS, whereas CHIP neither interacted with iNOS nor had any effects on the subcellular localization, ubiquitination, and proteasomal degradation of iNOS. These results differ from previous reports. Furthermore, the lifetime of the iNOS(N27A) mutant, a form of iNOS that does not bind to ECS(SPSB), was substantially extended in macrophages. These results demonstrate that ECS(SPSB), but not CHIP, is the master regulator of the iNOS lifetime.

1. Introduction

Nitric oxide (NO) is an important multifunctional biomolecule that is endogenously synthesized from L-arginine by NO synthases (NOSs) [1]. Inducible NOS (iNOS) is known to produce a relatively large amount of NO because of its Ca^{2+}-independent activity [1]. Excessive NO production via iNOS induces apoptotic cell death of activated macrophages [2] and is linked to numerous human pathologies, including asthma, arthritis, and endotoxin shock [3,4]. Thus, the lifetime of iNOS needs to be tightly regulated. iNOS is known to be degraded by the ubiquitin–proteasome pathway [5,6]. The two E3 ubiquitin ligases, Elongin B/C–Cullin-5–SPRY domain- and SOCS box-containing protein [ECS(SPSB)] and the C-terminus of Hsp70–interacting protein (CHIP), have been reported to target iNOS for proteasomal degradation [7–10]. However, the significance of each E3 ubiquitin ligase for the ubiquitination and proteasomal degradation of iNOS has not been clarified.

Because CHIP has been shown to promote ubiquitination and proteasomal degradation of non-native or misfolded proteins rather than native or properly folded proteins [11–17], CHIP is involved in the regulation of a wide range of proteins. In addition, CHIP has been shown to regulate neuronal NOS (nNOS) and endothelial NOS (eNOS) as well as iNOS [18,19]. In contrast, the specificity of ECS(SPSB) is strict, because SPSB proteins, the substrate recognition subunits of ECS(SPSB), recognize unique core sequences, D/E-I/L-N-N-N [20]. Only 11 mouse proteins and 16 human proteins contain this sequence [10], and currently iNOS is the only substrate identified for ECS(SPSB). Whether or not ECS(SPSB) regulates nNOS and eNOS is unknown.

In the present study, we investigated both the specificity of ECS(SPSB) for all NOS isoforms and the relative significance of ECS(SPSB) and CHIP for ubiquitination and proteasomal degradation of iNOS. Our findings suggest that ECS(SPSB), but not CHIP, is an iNOS-specific E3 ubiquitin ligase and is the master regulator of the iNOS lifetime.

Abbreviations: ECS, Elongin B/C–Cullin-5–SOCS box protein; SPSB, SPRY domain- and SOCS box-containing protein; ECS(SPSB), ECS containing SPSB as a SOCS box protein; NOS, nitric-oxide synthase; iNOS, inducible NOS; CHX, cycloheximide; YFP, yellow fluorescent protein.

* Corresponding author. Address: Department of Cellular Pharmacology, Hokkaido University Graduate School of Medicine, N15W7, Sapporo 060-8638, Japan.
E-mail address: nishiya@med.hokudai.ac.jp (T. Nishiya).

0006-291X/$ - see front matter © 2011 Elsevier Inc. All rights reserved.
doi:10.1016/j.bbrc.2011.04.103

2. Materials and methods

2.1. Reagents

Anti-Myc antibody was obtained from Cell Signaling Technology. Anti-FLAG (M2) antibody and anti-CHIP antibody were from Sigma. Anti-iNOS antibody was from Millipore. Anti-GAPDH antibody was from Santa Cruz Biotechnology. Anti-α-tubulin antibody was from Invitrogen. Anti-6× His-tag antibody was from MBL. Anti-GFP antibody (clone JL-8) was from Clontech. Cycloheximide (CHX) was from Calbiochem.

2.2. Cell culture

HEK293T cells were grown in Dulbecco's modified Eagle's medium (DMEM) containing 10% fetal bovine serum (FBS). HEK293T cells stably expressing myc-tagged ubiquitin (293T-^{myc}Ub cells [9]) were grown in DMEM containing 10% FBS and 1 μg/ml puromycin. RAW264.7 mouse macrophage cell line was grown in RPMI containing 10% FBS and 1 mM pyruvate.

2.3. cDNAs and plasmids

The cDNAs encoding full-length human iNOS (hiNOS), hnNOS and heNOS were subcloned into the pCMV-Tag5A vector (Stratagene). The plasmids for expressing hiNOS mutants (N26A, N27A, and N25–27A) were constructed by using the QuikChange™ Site-Direct Mutagenesis Kit (Stratagene) and pSG5-hiNOS vector as a template. The cDNAs encoding residues 1–263 (FL), 1–85 (N), 86–219 (SPRY), 220–263 (SOCS), 86–263 (ΔN), 1–85 fused to 220–263 (ΔSPRY), and 1–221 (ΔSOCS) of human SPSB2 (hSPSB2) were subcloned into the pGEX-6P-2 vector (GE Healthcare). The cDNAs encoding hiNOS and hiNOS(N27A) mutant were subcloned into the pMXrmv5-$(G_4S)_3$-YFP retroviral vector [21].

2.4. Co-immunoprecipitation

HEK293T cells in a 6-well plate were transfected with the indicated plasmids for 24 h. The cells were lysed in 500 μl of buffer A (50 mM Tris–HCl, 150 mM NaCl, 1% Nonidet P-40, 5 mM EDTA, and a protease inhibitor mixture (Roche), pH 7.5). The lysates were centrifuged at 20,000*g* for 10 min at 4 °C. The supernatants were pre-cleared with 40 μl of protein G-Sepharose 4FF beads (GE Healthcare) for 30 min. The pre-cleared lysates were incubated with the indicated antibodies for 16 h at 4 °C, and successively with 40 μl of protein G-Sepharose 4FF beads for 4 h at 4 °C. The beads were washed five times with 1 ml of buffer A. Immunoprecipitated proteins were eluted by boiling with 40 μl of 2× SDS–PAGE sample buffer for 5 min, and subjected to immunoblotting.

2.5. GST-pull down assay

GST fusion proteins were expressed in BL21-CodonPlus(DE3)-RILP bacteria (Stratagene) and were purified by using the Glutathione Sepharose 4B (GE Healthcare) as described previously [22].

HEK293T cells were transfected with pSG5-hiNOS. After 24 h, lysates were prepared, and the supernatants (200 μg proteins) were incubated with 5 μg of GST fusion proteins for 3 h at 4 °C. The GST fusion protein-bound beads were washed five times with buffer A, boiled with 75 μl of 2× SDS–PAGE sample buffer, and 12 μl of each sample was subjected to immunoblotting using anti-iNOS antibody.

2.6. Quantitation of nitrite in culture medium

The production of nitrite was measured using Griess reagent as described previously [23].

2.7. Detection of ubiquitinated iNOS

293T-^{myc}Ub cells in 6-well plates were washed with PBS and lysed with 1 ml buffer B (PBS containing 0.1% SDS, 0.5% deoxycholic acid, 1% Nonidet P-40, 0.5 mM EDTA, 5 mM *N*-ethylmaleimide, 1 mM NaF, and a protease inhibitor cocktail). The lysates were centrifuged at 20,000*g* for 20 min at 4 °C, and the supernatants were then pre-cleared with 50 μl protein G-Sepharose 4FF beads for 30 min, and centrifuged at 20,000*g* for 10 min at 4 °C. The pre-cleared lysates were incubated with 3 μg of anti-iNOS antibody for 90 min at 4 °C, and successively with 50 μl protein G-Sepharose 4FF beads for 90 min at 4 °C. The beads were washed five times with 1 ml buffer B. Immunoprecipitated proteins were eluted by boiling with 40 μl 2× SDS–PAGE sample buffer for 1 min, and subjected to immunoblotting.

2.8. Microscopy

HEK293T cells transfected with the indicated plasmids were placed into a glass bottom dish (IWAKI) coated with poly-L-lysine (Sigma). The next day, images were acquired using an Olympus IX-71 fluorescent microscope.

2.9. Expression of YFP fusion proteins in RAW264.7 macrophages

Introduction of genes into RAW264.7 macrophages was carried out by retroviral gene transfer as described previously [23].

3. Results

3.1. Neither nNOS nor eNOS are regulated by ECS(SPSB)

We have recently reported that the ECS E3 ubiquitin ligase containing SPSB1, SPSB2, or SPSB4 as a SOCS box protein (ECS(SPSB)) targets iNOS for proteasomal degradation [9]. The SPSB recognition sequence (DINNN) is present in the N-terminal region of iNOS (amino acids 23–27) [10,20]. The N-terminal region located before the oxygenase domain of three NOS isoforms contains a domain or motif that is unique to each NOS isoform and thus endows each NOS isoform with specific biochemical and physiological features [24,25]. To examine whether ECS(SPSB) specifically regulates iNOS, we compared the amino acid sequence of N-terminal regions of three NOS isoforms and found that the DINNN motif is conserved in iNOS proteins from various animals (data not shown), but is not present in either nNOS or eNOS (Fig. 1A). Consistent with this finding, iNOS interacted with SPSB2 (Fig. 1B) and was rapidly degraded in the presence of SPSB1 (Fig. 1C), whereas neither nNOS nor eNOS interacted with SPSB2 and were degraded despite SPSB1 expression. These results demonstrate that ECS(SPSB) specifically regulates iNOS.

The authors have previously reported that asparagine 27 of iNOS is a key residue for interactions with SPSB1, SPSB2, and SPSB4 [9,10]. However, it remains unclear which part of SPSB is involved in the interaction with iNOS. To map the iNOS binding site on SPSB, we generated selective deletions of the SPSB2 sequence (Fig. 1D), and analyzed the interaction with iNOS by GST pull-down assays. We found that the entire molecule, except the SOCS box, is required for the interaction with iNOS, although the SPRY domain alone faintly bound to iNOS (Fig. 1E).

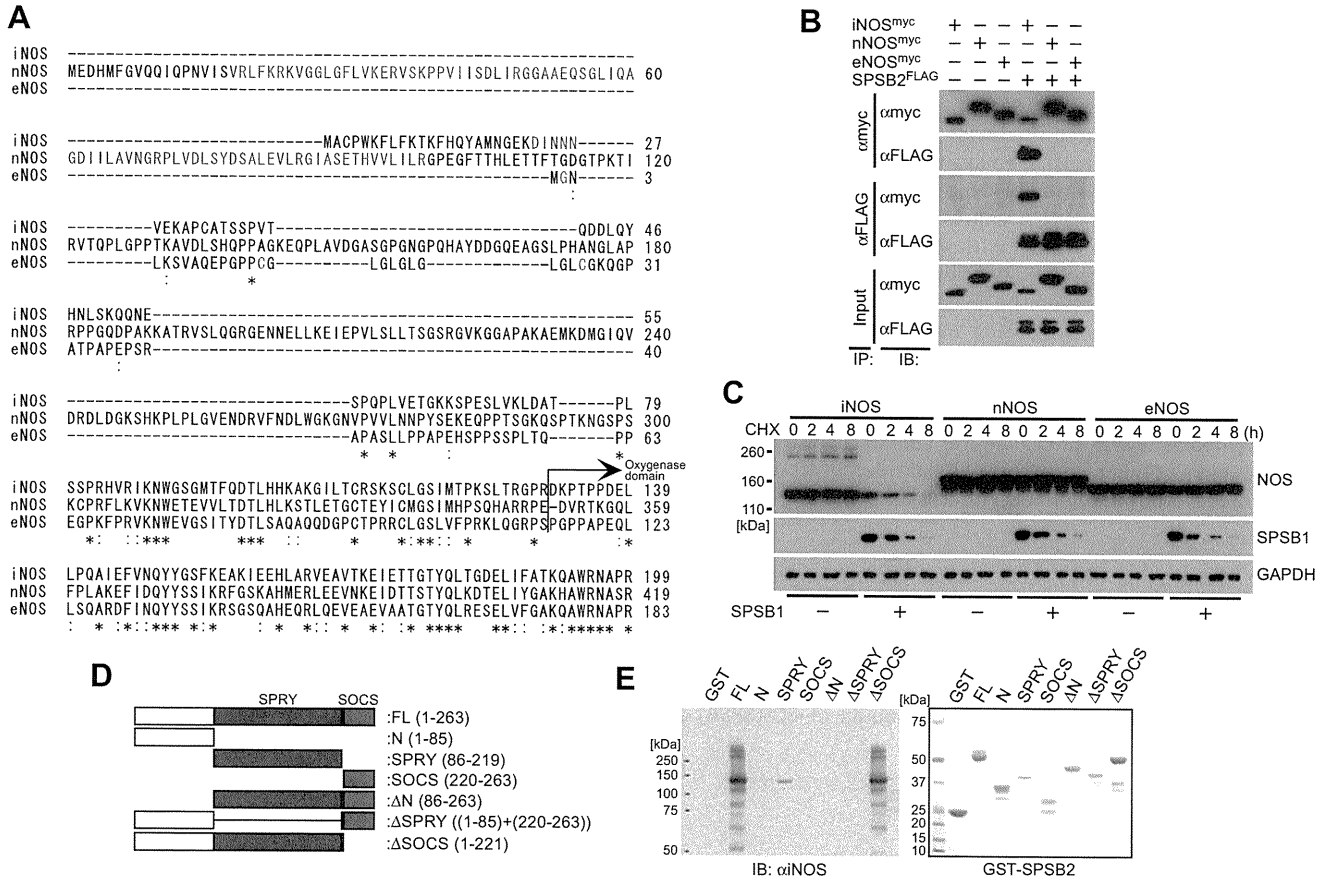

Fig. 1. iNOS, but not nNOS and eNOS, interacts with ECS(SPSB) and is rapidly degraded by ECS(SPSB). (A) Alignment of amino acid residues at the N-terminal region of NOSs. Amino acid residues at the N-terminal region of human iNOS (GenBank: AAI30284), human nNOS (GenBank: NP_000611), and human eNOS (GenBank: ABY87544) were aligned by introducing gaps (–) to obtain maximum homology. The SPSB recognition motif in iNOS is shown in red, the PDZ domain in nNOS is shown in green, and both the myristoylation site (Gly-2) and palmitoylation sites (Cys-15 and -26) in eNOS are shown in orange. A colon indicates amino acid similarity and a star indicates amino acid identity. (B) Interactions between SPSB2 and three NOS isoforms. HEK293T cells in 6-well plate were transfected with expression plasmids for FLAG-tagged SPSB2 (1 μg) and myc-tagged NOS isoforms (0.5 μg) for 24 h. The empty vector was also transfected to ensure that a total of 4 μg of DNA was used per transfection. The cell lysates were prepared and subjected to immunoprecipitation and immunoblotting. (C) HEK293T cells in 6-well plate were transfected with expression plasmids for FLAG-tagged SPSB1 (1 μg) and myc-tagged NOS isoforms (0.75 μg) for 12 h. The empty vector was also transfected to ensure that a total of 4 μg of DNA was used per transfection. Then the cells were placed into 4 wells of a 24-well plate. After 12 h, the cells were treated with 100 μM CHX for the indicated periods. The cell lysates were prepared and subjected to immunoblotting. (D) A schematic representation of SPSB2 mutants. (E) An immunoblot of an iNOS pull-down with various GST-tagged SPSB2 fragments bound to Glutathione Sepharose 4B (left panel). The amounts of each GST-tagged SPSB2 fragment were estimated from Coomassie blue staining (right panel).

3.2. ECS(SPSB), but not CHIP, regulates the subcellular redistribution and proteasomal degradation of iNOS

CHIP is the first E3 ubiquitin ligase that has been reported to promote the ubiquitination and proteasomal degradation of iNOS [7,8]. To determine which E3 ubiquitin ligase, ECS(SPSB) or CHIP, is essential for iNOS regulation, we examined the down-regulation of iNOS levels when SPSB1 or CHIP was co-expressed. We found that both the iNOS level and NO production via iNOS were substantially decreased when SPSB1 was co-expressed, whereas the co-expression of CHIP affected neither the iNOS level nor NO production via iNOS (Fig. 2 A and B), which differs from previous observations [7,8]. We next examined the stability of iNOS proteins in cycloheximide (CHX) chase assays [26]. We found that SPSB1 triggered iNOS degradation, and in particular, that the much lower expression of SPSB1 induced more rapid degradation of iNOS (Fig. 2C), consistent with our previous report [9]. In contrast, CHIP did not induce the degradation of iNOS, though CHIP down-regulated the basal levels of all proteins tested, especially GAPDH, in a dose-dependent manner.

Next, we examined the interactions of iNOS with SPSB1 and CHIP. FLAG-tagged SPSB1 and 6× His-tagged CHIP were expressed together with iNOS in HEK293T cells, and then those proteins were immunoprecipitated with antibodies for iNOS, FLAG-tag, and 6× His-tag. Co-immunoprecipitation with each protein was determined by immunoblotting. We found that SPSB1 was co-immunoprecipitated with iNOS in anti-iNOS immunoprecipitants (Fig. 2D, lane 5) and iNOS was also co-immunoprecipitated with SPSB1 in anti-FLAG immunoprecipitants (Fig. 2E), suggesting that iNOS interacts with SPSB1. In contrast, the interaction between iNOS and CHIP was not detected in either anti-iNOS or anti-6× His-tag immunoprecipitants (Fig. 2 D and F). Although a faint signal was seen under overexposure conditions on an anti-CHIP immunoblot for anti-iNOS immunoprecipitants (Fig. 2D, lane 6), it was uncertain whether this signal was derived from CHIP or not, because a similar signal was also observed in control IgG immunoprecipitants (Fig. 2D, lanes 1–3). Consistent with the fact that CHIP was originally identified as a protein interacting with Hsp70 [17], we found that endogenous Hsp70 was co-immunoprecipitated with 6× His-tagged CHIP in anti-6× His-tag immunoprecipitants (Fig. 2F), suggesting that 6× His-tagged CHIP functioned properly.

Given that we have recently reported that SPSB1, SPSB2, and SPSB4 can induce the subcellular redistribution of iNOS from dense regions to diffused expression [9], we next examined whether the

subcellular localization of iNOS is affected by CHIP. As shown in Fig. 2G, the subcellular localization of C-terminal yellow fluorescent protein (YFP)-tagged iNOS was unaffected by the co-expression of CHIP.

Finally, we investigated the levels of ubiquitinated iNOS when SPSB1 or CHIP was expressed. To evaluate the level of ubiquitinated iNOS, HEK293T cells stably expressing myc-tagged ubiquitin were transfected with cDNAs expressing iNOS, SPSB1, and CHIP for 24 h, followed by treatment with MG-132 for 4 h to accumulate ubiquitinated proteins. iNOS was immunoprecipitated with an anti-iNOS antibody and then the levels of ubiquitinated iNOS were analyzed by immunoblotting using an anti-myc antibody. We confirmed the expression of transfected iNOS, SPSB1, and CHIP by immunoblotting (Fig. 3A). We found that the level of ubiquitinated iNOS was enhanced more than 3-fold in cells transfected with SPSB1, whereas it was unchanged in cells transfected with CHIP (Fig. 3B and C). Taken together, our data demonstrate that CHIP is not involved in the regulation of iNOS.

3.3. The lifetime of the iNOS(N27A) mutant is much longer than that of wild-type iNOS in macrophages

Because the iNOS(N27A) mutant, a form of iNOS that does not bind to ECS(SPSB), is completely resistant to the protein degradation mediated by ECS(SPSB) [9], the amounts of ECS(SPSB) and CHIP critical for the proteasomal degradation of iNOS could be determined by the degree of degradation of the iNOS(N27A) mutant. Thus, we examined the degradation rates of wild-type iNOS and the iNOS(N27A) mutant in RAW264.7 macrophages, in which endogenous SPSB1, SPSB2, and CHIP are expressed [8,9]. YFP, iNOS–YFP, or the iNOS(N27A)–YFP were retrovirally expressed in RAW264.7 macrophages and the stabilities of those proteins were examined in a CHX chase assays. Approximately 80% of iNOS–YFP was degraded within 4 h after CHX treatment, whereas approximately 70% of the iNOS(N27A)-YEP was still present 8 h after CHX treatment (Fig. 4A), with a similar kinetic of degradation of YFP alone (Fig. 4B). These data suggest that the ECS(SPSB) E3 ubiquitin ligase is the master regulator of the iNOS lifetime in macrophages.

4. Discussion

We performed experiments to investigate whether ECS(SPSB) specifically regulates iNOS among all NOS isoforms, and to determine the degree to which ECS(SPSB) and CHIP are fundamental to iNOS regulation. Our results show that ECS(SPSB) binding is iNOS-specific, and ECS(SPSB) targets iNOS, but not nNOS and eNOS, for proteasomal degradation. In addition, the lifetime of the iNOS(N27A) mutant, a form of iNOS not bound to ECS(SPSB), is substantially extended in macrophages. In contrast, CHIP had

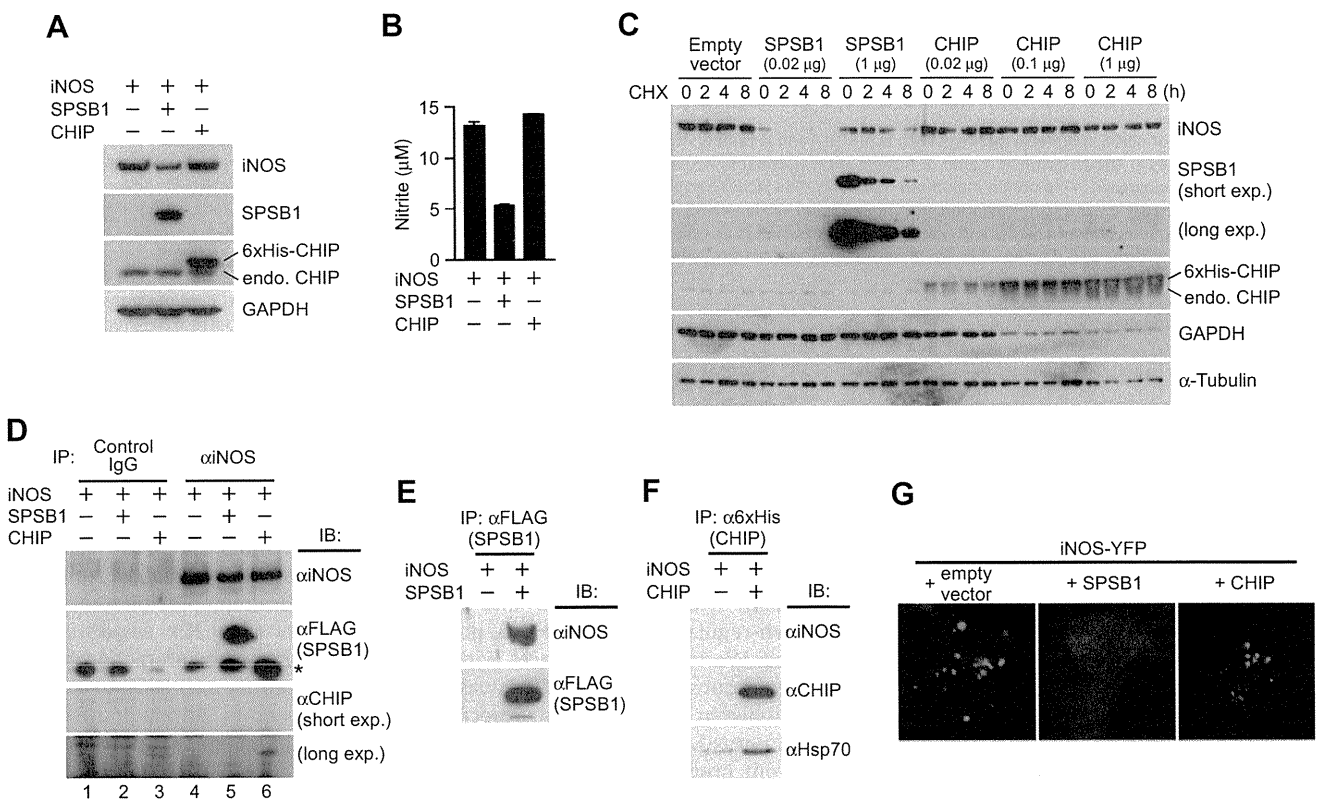

Fig. 2. ECS(SPSB), but not CHIP, regulates the subcellular redistribution and proteasomal degradation of iNOS (A) and (B), HEK293T cells in 6-well plates were transfected with expression plasmids for iNOS (2 μg) and FLAG-tagged SPSB1 (0.25 μg) or 6× His-tagged CHIP (0.25 μg) for 24 h. The empty vector was also transfected to ensure that a total of 4 μg of DNA was used per transfection. Then, the cell lysates were prepared, and subjected to immunoblotting using anti-iNOS, anti-FLAG, anti-CHIP, and anti-GAPDH antibodies. The concentration of nitrite in the cell culture medium was assessed by the Griess assay (B). Data are presented as mean ± standard deviation (SD), $n = 3$. (C) HEK293T cells in 6-well plates were transfected with expression plasmids for iNOS (2 μg) and FLAG-tagged SPSB1 (0.02 and 1 μg) or 6× His-tagged CHIP (0.02, 0.1, and 1 μg) for 12 h. The empty vector was also transfected to ensure that a total of 4 μg of DNA was used per transfection and the cells were placed into 4 wells of 24-well plate. After 12 h, the cells were treated with 100 μM CHX for the indicated periods. The cell lysates were prepared and subjected to immunoblotting. (D–F) The lysates from A (800 μg proteins) were subjected to immunoprecipitation and immunoblotting. A star indicates the light chain of the antibody. (G) In 12-well plates, HEK293T cells were transfected with expression plasmids for iNOS–YFP (1 μg) and FLAG-tagged SPSB1 (0.1 μg) or 6× His-tagged CHIP (0.1 μg) for 12 h. The empty vector was also transfected to ensure that a total of 1.6 μg of DNA was used per transfection. The cells were then placed into a 35 mm glass bottom dish. The next day, the subcellular localization of iNOS–YFP proteins was examined by fluorescence microscopy.

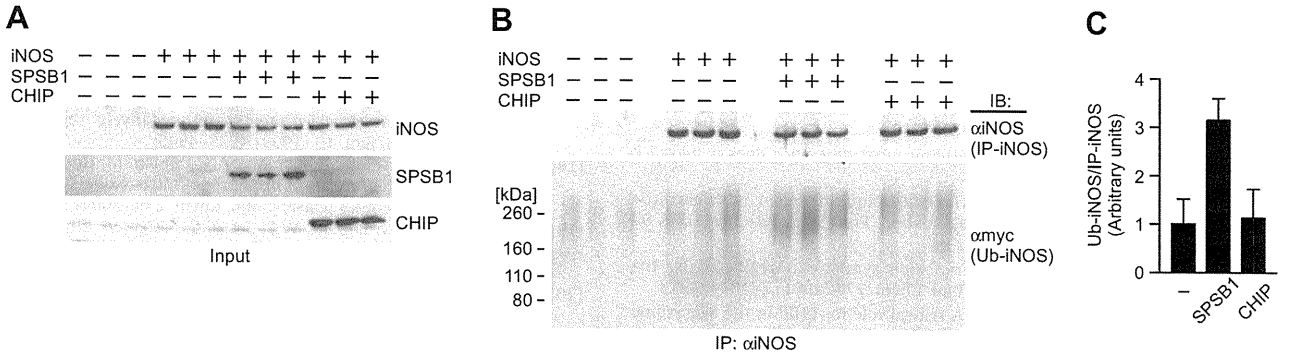

Fig. 3. ECS(SPSB), but not CHIP, induces the ubiquitination of iNOS. (A, B) In 6-well plates, 293T-^{myc}Ub cells were transfected with expression plasmids for iNOS (2 μg) and FLAG-tagged SPSB1 (0.1 μg) or 6× His-tagged CHIP (0.1 μg) for 24 h followed by treatment with 5 μM MG-132 for 4 h. A portion of each cell lysate was subjected to immunoblotting (A). The remaining cell lysate was subjected to immunoprecipitation using an anti-iNOS antibody, and the ubiquitinated iNOS was analyzed by immunoblotting using an anti-myc antibody (B). Each sample was prepared and loaded in triplicate. (C) The quantification of the levels of ubiquitinated iNOS shown in (B). Data represent mean ± SD, $n = 3$.

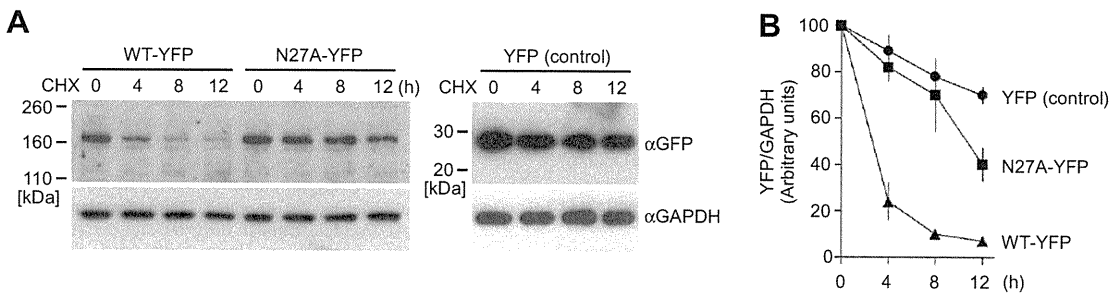

Fig. 4. The lifetime of the iNOS(N27A) mutant, a form of iNOS that does not bind to ECS(SPSB), is significantly extended in macrophages. (A) RAW264.7 macrophages were infected with retroviruses carrying YFP alone, iNOS–YFP, or the iNOS(N27A)-YFP. After 12 h, the cells were placed into 4 wells of 24-well plate. After 12 h, the cells were treated with 100 μM CHX for the indicated periods. The cell lysates were prepared and subjected to immunoblotting. (B) The quantification of the levels of YFP, iNOS–YFP, and the iNOS(N27A)-YFP shown in (A). Data represent mean ± SD, $n = 3$.

absolutely no effect on the regulation of iNOS. These results demonstrate that ECS(SPSB), but not CHIP, is an essential E3 ubiquitin ligase for the regulation of the iNOS lifetime.

Eissa et al. first reported the ubiquitin/proteasome-dependent degradation of iNOS [5,6,27]. Furthermore, Eissa et al. as well as Yin et al. independently reported that CHIP facilitates the ubiquitination and proteasomal degradation of iNOS [7,8]. In addition, we, along with Nicholson et al. recently reported that ECS(SPSB) targets iNOS for proteasomal degradation [9,10]. In contrast to the previous reports by Eissa et al. and Yin et al., in the present study we did not see any effects of CHIP on iNOS regulation in terms of the interaction with iNOS, the subcellular redistribution of iNOS, and ubiquitin/proteasome-dependent degradation of iNOS. Many reports have demonstrated that CHIP promotes ubiquitination and proteasomal degradation of non-native or misfolded proteins, rather than native or properly folded proteins [11–17]. The previous findings that CHIP mediated the proteasomal degradation of iNOS may have resulted from the expression of iNOS proteins as misfolded proteins in the respective experimental systems. In this study, iNOS was expressed in HEK293T cells by transfection with pSG5–hiNOS plasmid at physiological levels, because the iNOS levels expressed by this plasmid were quite similar to those expressed in RAW264.7 macrophages stimulated with 10 ng/ml LPS for 24 h (data not shown). In this case, most iNOS proteins are present in detergent soluble fractions (data not shown). It is possible that the previous studies used iNOS expression constructs that carry much stronger promoters, and therefore a portion of the iNOS proteins were misfolded and recognized as such by CHIP.

Currently, iNOS is the only substrate identified for ECS(SPSB). SPSB1, SPSB2, and SPSB4 recognize unique core sequences, D/E-I/L-N-N-N [20,28]. We performed a BLAST search to search for any proteins containing those sequences. A total of 17 human proteins were identified, only 4 of which contain those sequences across species, suggesting that ECS(SPSB) functions mainly to maintain appropriate iNOS levels through the ubiquitin/proteasome-dependent degradation of iNOS to prevent overproduction of NO during iNOS induction. Further studies using iNOS(N27A) knock-in mice may more clearly determine the significance of ECS(SPSB) E3 ubiquitin ligase in the regulation of the iNOS lifetime.

Conflict of interest

None.

Acknowledgments

We thank P.A. Marsden for plasmid encoding human nNOS, J.K. Liao for human eNOS, and L. Neckers for human CHIP. This research was supported in part by Grants-in-Aid for Scientific Research (C) (to T.N.) and (B) (to S.M.) from the Japan Society for the Promotion of Science, a Grant-in-Aid for Scientific Research on Innovative Areas (research in a proposed research area) from the Ministry of Education, Culture, Sports, Science and Technology (to T.U.), a Grant-in-Aid for Scientific Research from the Ministry of Health, Labour, and Welfare of Japan (to K.O.), the Smoking Research Foundation, Japan (to S.M.), the Northtec Foundation (to T.N.), and the Takeda Science Foundation (to T.N.).

References

[1] O.W. Griffith, D.J. Stuehr, Nitric oxide synthases: properties and catalytic mechanism, Annu. Rev. Physiol 57 (1995) 707–736.

[2] J.E. Albina, S. Cui, R.B. Mateo, J.S. Reichner, Nitric oxide-mediated apoptosis in murine peritoneal macrophages, J. Immunol. 150 (1993) 5080–5085.
[3] F.H. Guo, S.A. Comhair, S. Zheng, R.A. Dweik, N.T. Eissa, M.J. Thomassen, W. Calhoun, S.C. Erzurum, Molecular mechanisms of increased nitric oxide (NO) in asthma: evidence for transcriptional and post-translational regulation of NO synthesis, J. Immunol. 164 (2000) 5970–5980.
[4] C. Nathan, Inducible nitric oxide synthase: what difference does it make? J. Clin. Invest. 100 (1997) 2417–2423.
[5] P.J. Kolodziejski, A. Musial, J.S. Koo, N.T. Eissa, Ubiquitination of inducible nitric oxide synthase is required for its degradation, Proc. Natl. Acad. Sci. USA 99 (2002) 12315–12320.
[6] A. Musial, N.T. Eissa, Inducible nitric-oxide synthase is regulated by the proteasome degradation pathway, J. Biol. Chem. 276 (2001) 24268–24273.
[7] Y. Sha, L. Pandit, S. Zeng, N.T. Eissa, A critical role for CHIP in the aggresome pathway, Mol. Cell. Biol. 29 (2009) 116–128.
[8] L. Chen, X. Kong, J. Fu, Y. Xu, S. Fang, P. Hua, L. Luo, Z. Yin, CHIP facilitates ubiquitination of inducible nitric oxide synthase and promotes its proteasomal degradation, Cell. Immunol. 258 (2009) 38–43.
[9] T. Nishiya, K. Matsumoto, S. Maekawa, E. Kajita, T. Horinouchi, M. Fujimuro, K. Ogasawara, T. Uehara, S. Miwa, Regulation of inducible nitric oxide synthase by the SPRY domain- and SOCS box-containing proteins, J. Biol. Chem. 286 (2011) 9009–9019.
[10] Z. Kuang, R.S. Lewis, J.M. Curtis, Y. Zhan, B.M. Saunders, J.J. Babon, T.B. Kolesnik, A. Low, S.L. Masters, T.A. Willson, L. Kedzierski, S. Yao, E. Handman, R.S. Norton, S.E. Nicholson, The SPRY domain-containing SOCS box protein SPSB2 targets iNOS for proteasomal degradation, J. Cell Biol. 190 (2010) 129–141.
[11] H.S. Ko, R. Bailey, W.W. Smith, Z. Liu, J.H. Shin, Y.I. Lee, Y.J. Zhang, H. Jiang, C.A. Ross, D.J. Moore, C. Patterson, L. Petrucelli, T.M. Dawson, V.L. Dawson, CHIP regulates leucine-rich repeat kinase-2 ubiquitination, degradation, and toxicity, Proc. Natl. Acad. Sci. USA 106 (2009) 2897–2902.
[12] M.F. Rosser, E. Washburn, P.J. Muchowski, C. Patterson, D.M. Cyr, Chaperone functions of the E3 ubiquitin ligase CHIP, J. Biol. Chem. 282 (2007) 22267–22277.
[13] D.M. Cyr, J. Hohfeld, C. Patterson, Protein quality control: U-box-containing E3 ubiquitin ligases join the fold, Trends Biochem. Sci. 27 (2002) 368–375.
[14] S. Murata, Y. Minami, M. Minami, T. Chiba, K. Tanaka, CHIP is a chaperone-dependent E3 ligase that ubiquitylates unfolded protein, EMBO Rep. 2 (2001) 1133–1138.
[15] G.C. Meacham, C. Patterson, W. Zhang, J.M. Younger, D.M. Cyr, The Hsc70 co-chaperone CHIP targets immature CFTR for proteasomal degradation, Nat. Cell Biol. 3 (2001) 100–105.
[16] P. Connell, C.A. Ballinger, J. Jiang, Y. Wu, L.J. Thompson, J. Hohfeld, C. Patterson, The co-chaperone CHIP regulates protein triage decisions mediated by heat-shock proteins, Nat. Cell Biol. 3 (2001) 93–96.
[17] C.A. Ballinger, P. Connell, Y. Wu, Z. Hu, L.J. Thompson, L.Y. Yin, C. Patterson, Identification of CHIP, a novel tetratricopeptide repeat-containing protein that interacts with heat shock proteins and negatively regulates chaperone functions, Mol. Cell. Biol. 19 (1999) 4535–4545.
[18] H.M. Peng, Y. Morishima, G.J. Jenkins, A.Y. Dunbar, M. Lau, C. Patterson, W.B. Pratt, Y. Osawa, Ubiquitylation of neuronal nitric-oxide synthase by CHIP, a chaperone-dependent E3 ligase, J. Biol. Chem. 279 (2004) 52970–52977.
[19] J. Jiang, D. Cyr, R.W. Babbitt, W.C. Sessa, C. Patterson, Chaperone-dependent regulation of endothelial nitric-oxide synthase intracellular trafficking by the co-chaperone/ubiquitin ligase CHIP, J. Biol. Chem. 278 (2003) 49332–49341.
[20] J.S. Woo, H.Y. Suh, S.Y. Park, B.H. Oh, Structural basis for protein recognition by B30.2/SPRY domains, Mol. Cell 24 (2006) 967–976.
[21] T. Nishiya, E. Kajita, S. Miwa, A.L. Defranco, TLR3 and TLR7 are targeted to the same intracellular compartments by distinct regulatory elements, J. Biol. Chem. 280 (2005) 37107–37117.
[22] T. Nishiya, E. Kajita, T. Horinouchi, A. Nishimoto, S. Miwa, Distinct roles of TIR and non-TIR regions in the subcellular localization and signaling properties of MyD88, FEBS Lett. 581 (2007) 3223–3229.
[23] T. Nishiya, A.L. DeFranco, Ligand-regulated chimeric receptor approach reveals distinctive subcellular localization and signaling properties of the Toll-like receptors, J. Biol. Chem. 279 (2004) 19008–19017.
[24] J.E. Brenman, D.S. Chao, S.H. Gee, A.W. McGee, S.E. Craven, D.R. Santillano, Z. Wu, F. Huang, H. Xia, M.F. Peters, S.C. Froehner, D.S. Bredt, Interaction of nitric oxide synthase with the postsynaptic density protein PSD-95 and alpha1-syntrophin mediated by PDZ domains, Cell 84 (1996) 757–767.
[25] P. Prabhakar, V. Cheng, T. Michel, A chimeric transmembrane domain directs endothelial nitric-oxide synthase palmitoylation and targeting to plasmalemmal caveolae, J. Biol. Chem. 275 (2000) 19416–19421.
[26] N. Shembade, N.S. Harhaj, K. Parvatiyar, N.G. Copeland, N.A. Jenkins, L.E. Matesic, E.W. Harhaj, The E3 ligase Itch negatively regulates inflammatory signaling pathways by controlling the function of the ubiquitin-editing enzyme A20, Nat. Immunol. 9 (2008) 254–262.
[27] P.J. Kolodziejski, J.S. Koo, N.T. Eissa, Regulation of inducible nitric oxide synthase by rapid cellular turnover and cotranslational down-regulation by dimerization inhibitors, Proc. Natl. Acad. Sci. USA 101 (2004) 18141–18146.
[28] P. Filippakopoulos, A. Low, T.D. Sharpe, J. Uppenberg, S. Yao, Z. Kuang, P. Savitsky, R.S. Lewis, S.E. Nicholson, R.S. Norton, A.N. Bullock, Structural basis for Par-4 recognition by the SPRY domain- and SOCS box-containing proteins SPSB1, SPSB2, and SPSB4, J. Mol. Biol. 401 (2010) 389–402.

On–off system for PI3-kinase–Akt signaling through *S*-nitrosylation of phosphatase with sequence homology to tensin (PTEN)

Naoki Numajiri[a,1], Kumi Takasawa[a,1], Tadashi Nishiya[b,1], Hirotaka Tanaka[c], Kazuki Ohno[d], Wataru Hayakawa[a], Mariko Asada[a], Hiromi Matsuda[a], Kaoru Azumi[e], Hideaki Kamata[f], Tomohiro Nakamura[g], Hideaki Hara[c], Masabumi Minami[a], Stuart A. Lipton[g], and Takashi Uehara[a,d,2]

Departments of [a]Pharmacology and [e]Biochemistry, Graduate School of Pharmaceutical Sciences, Hokkaido University, Sapporo 060-0812, Japan; [b]Department of Cellular Pharmacology, Graduate School of Medicine, Hokkaido University, Sapporo 060-8636, Japan; [c]Molecular Pharmacology, Department of Biofunctional Evaluation, Gifu Pharmaceutical University, Gifu 501-1196, Japan; [d]Department of Medicinal Pharmacology, Graduate School of Medicine, Dentistry and Pharmaceutical Sciences, Okayama University, Okayama 700-8530, Japan; [f]Laboratory of Biomedical Chemistry, Department of Molecular Medical Sciences, Graduate School of Biomedical Science, Hiroshima University, Hiroshima 734-8553, Japan; and [g]Del E. Webb Center for Neuroscience, Aging, and Stem Cell Research, Sanford-Burnham Medical Research Institute, La Jolla, CA 92037

Edited by Solomon H. Snyder, Johns Hopkins University School of Medicine, Baltimore, MD, and approved May 17, 2011 (received for review March 4, 2011)

Nitric oxide (NO) physiologically regulates numerous cellular responses through *S*-nitrosylation of protein cysteine residues. We performed antibody-array screening in conjunction with biotin-switch assays to look for *S*-nitrosylated proteins. Using this combination of techniques, we found that phosphatase with sequence homology to tensin (PTEN) is selectively *S*-nitrosylated by low concentrations of NO at a specific cysteine residue (Cys-83). *S*-nitrosylation of PTEN (forming SNO-PTEN) inhibits enzymatic activity and consequently stimulates the downstream Akt cascade, indicating that Cys-83 is a critical site for redox regulation of PTEN function. In ischemic mouse brain, we observed SNO-PTEN in the core and penumbra regions but found SNO-Akt, which is known to inhibit Akt activity, only in the ischemic core. These findings suggest that low concentrations of NO, as found in the penumbra, preferentially *S*-nitrosylate PTEN, whereas higher concentrations of NO, known to exist in the ischemic core, also *S*-nitrosylate Akt. In the penumbra, inhibition of PTEN (but not Akt) activity by *S*-nitrosylation would be expected to contribute to cell survival by means of enhanced Akt signaling. In contrast, in the ischemic core, SNO-Akt formation would inhibit this neuroprotective pathway. In vitro model systems support this notion. Thus, we identify unique sites of PTEN and Akt regulation by means of *S*-nitrosylation, resulting in an "on–off" pattern of control of Akt signaling.

apoptosis | ischemia | oxidation

Nitric oxide (NO) exerts pleiotropic cellular responses on proliferation, apoptosis, neurotransmission, and neurotoxicity in several types of cells by means of protein *S*-nitrosylation. This modification occurs by means of oxidative reaction between NO and cysteine (Cys) thiol in the presence of an electron acceptor (such as O_2 or a transition metal) or through transnitrosylation from *S*-nitrosothiol to another Cys thiol (1–3). Several methods have been published to detect *S*-nitrosylated proteins (SNO-Ps) by using antibodies, photolysis, and mercury affinity (4). In particular, the biotin-switch assay is a modified immunoblot developed by Jaffrey and Snyder that has been commonly used to detect endogenous SNO-Ps; this method has greatly advanced the field (5). Subsequently, other methods have been developed to detect SNO-Ps (6), but some of them involve samples treated with high concentrations of NO donor. In the presence of high concentrations of NO, however, it is possible that some Cys residues are artifactually *S*-nitrosylated.

Antibody arrays have been used to profile protein expression levels with high sensitivity. Each spotted antibody can be validated for its ability to bind proteins in the assay. Samples hybridizing to each antibody on the array can be easily detected. Although a number of proteins have been identified as substrates for *S*-nitrosylation in the past several years (3–6), we hypothesized that many more candidates modified by physiological levels of NO might still remain to be identified. We therefore tested whether an antibody array might be adapted for identification of additional SNO-Ps and their (patho)physiological functions.

In the present study, we attempted to isolate SNO-Ps in physiological condition by an antibody array. We prepared extracts from cells treated or untreated with NO and specifically labeled with biotin. We found that phosphatase with sequence homology to tensin (PTEN) is preferentially *S*-nitrosylated by low concentrations of NO. Although other reports have shown that PTEN can undergo *S*-nitrosylation by high concentrations of NO (7–13), here we found a significance of the (patho)physiological function of *S*-nitrosylated PTEN (SNO-PTEN) on the Akt pathway using in vivo and in vitro systems. Our results suggest that inhibition of PTEN activity through *S*-nitrosylation augments Akt signaling, thereby contributing to cell survival in ischemic brains and activation of endothelial NO synthase (eNOS).

Results

Screening for *S*-Nitrosylated Neural Proteins. Initially, we developed a unique screening system for isolating previously undescribed SNO-Ps in neuronal systems using an antibody array. Samples were prepared from human neuroblastoma SH-SY5Y cells that had been exposed to calcium ionophore A23187, which activates endogenous neuronal NO synthase (nNOS) and eNOS to produce physiological concentrations of NO. *S*-nitrosylated Cys residues in cell lysates were converted to their biotinylated form by using the biotin-switch technique (5). These samples, containing biotinylated cysteines, were subjected to antibody array, and fluorescent intensities were detected (Fig. S1). Twenty-five candidates were identified, including known SNO-Ps such as caspase, NOS, and HDAC (Table S1; refs. 14–16). Among the other candidates, we focused on the effect of *S*-nitrosylation on PTEN activity and its physiological functions. PTEN is an inhibitory regulator of the PI3-kinase/Akt signaling pathway, thereby attenuating cell growth, migration, and survival (17–21).

Author contributions: T.U. designed research; N.N., K.T., T. Nishiya, H.T., K.O., W.H., M.A., H.M., K.A., H.K., T. Nakamura, and T.U. performed research; N.N., K.T., T. Nishiya, K.A., H.H., M.M., S.A.L., and T.U. analyzed data; and S.A.L. and T.U. wrote the paper.

The authors declare no conflict of interest.

This article is a PNAS Direct Submission.

[1]N.N., K.T., and T. Nishiya contributed equally to this work.

[2]To whom correspondence should be addressed. E-mail: uehara@pharm.okayama-u.ac.jp.

This article contains supporting information online at www.pnas.org/lookup/suppl/doi:10.1073/pnas.1103503108/-/DCSupplemental.

S-Nitrosylation of PTEN. To validate *S*-nitrosylation of PTEN, we examined whether PTEN was significantly *S*-nitrosylated by a low concentration of the physiological NO donor *S*-nitrosocysteine (SNOC). SNOC markedly enhanced the level of SNO-PTEN in cell lysates and intact cells. SNO-PTEN was not detected in control biotin-switch assays performed without ascorbate to remove NO, thus preventing replacement of NO by biotin (Fig. 1*A*). As expected, PTEN was highly sensitive to NO; SNO-PTEN formation was detected in human embryonic kidney (HEK) 293 cells after treatment with 1–10 μM SNOC (Fig. 1 *B* and *C*). Furthermore, this modification was also found in cells exposed to various other types of NO donors, including *S*-nitroso-glutathione (GSNO) and 2-(*N*,*N*-diethylamino)-diazenolate-2-oxide (DETA-NONOate; Fig. S2).

Next, to investigate whether endogenously generated NO also induces SNO-PTEN formation, we used HEK cells stably expressing nNOS. PTEN was *S*-nitrosylated by endogenous NO in response to A23187 in a NOS-inhibitor–sensitive manner (Fig. 1*D* and Fig. S3). Mammalian PTEN has five cysteines in its phosphatase domain (17). To determine the target site of *S*-nitrosylation on PTEN, we mutated each cysteine to serine and assayed for SNO-PTEN formation using the biotin-switch method. HEK cells were transfected with expression vectors encoding either wild-type (WT) FLAG-PTEN or mutant forms of the protein. After 24 h, cells were exposed to SNOC or control conditions and monitored for SNO-PTEN. We found that C83S mutant PTEN produced almost no signal, suggesting that Cys-83 was the predominant *S*-nitrosylation site (Fig. 1*E*). Furthermore, we performed a chemical assay on purified recombinant PTEN to detect *S*-nitrosylation using 2,3-diaminonaphthalene (DAN). DAN stoichiometrically converts to fluorescent 2,3-naphthyltriazole in the presence of NO released from *S*-nitrosothiol. SNOC-treated PTEN resulted in significant SNO-P formation, whereas the PTEN(C83S) mutant was completely devoid of fluorescent signal (Fig. S3).

PTEN is known to be oxidized by high concentrations of H_2O_2 (>0.5 mM), which result in disulfide bond formation between Cys-71 and active site Cys-124 (22). Thus, we tested whether NO also induced disulfide bond formation in PTEN. However, even high concentrations of NO did not result in disulfide formation (Fig. 1*F*), consistent with the notion that *S*-nitrosylation of PTEN occurred solely at Cys-83. Thus, disparate Cys residues appear to be involved in *S*-nitrosylation and H_2O_2-mediated oxidation of PTEN.

SNO-PTEN Inhibits Phosphatase Activity Through C83. To determine whether *S*-nitrosylation affected PTEN activity, we initially monitored recombinant PTEN enzyme activity. Phosphatase activity was evaluated with a standard assay by measuring phosphate released from phosphatidylinositol-3,4,5-trisphosphate [PI(3,4,5)P3], a physiological substrate (23). Exposure of recombinant PTEN to SNOC significantly decreased the level of phosphate in a dose-dependent manner (Fig. 2*A*). This decline was reversed to basal levels after incubation with the chemical-reducing agent DTT, indicating that *S*-nitrosylation in PTEN was reversible (Fig. 2*B*). Next, we assessed the enzymatic activity of WT recombinant PTEN and Cys mutants. Cys-124 is essential for PTEN activity; thus, even in the absence of SNOC exposure, the C124S mutant completely lost its enzyme activity (Fig. 2*C*). In contrast, the C83S mutant maintained its enzymatic activity even after exposure to high concentrations of SNOC (Fig. 2*C*). Therefore, we made the observation that not only is Cys-83 the principal target site for PTEN oxidation by *S*-nitrosylation, but that this modification influences enzymatic activity by a mechanism distinct from that of oxidation by H_2O_2.

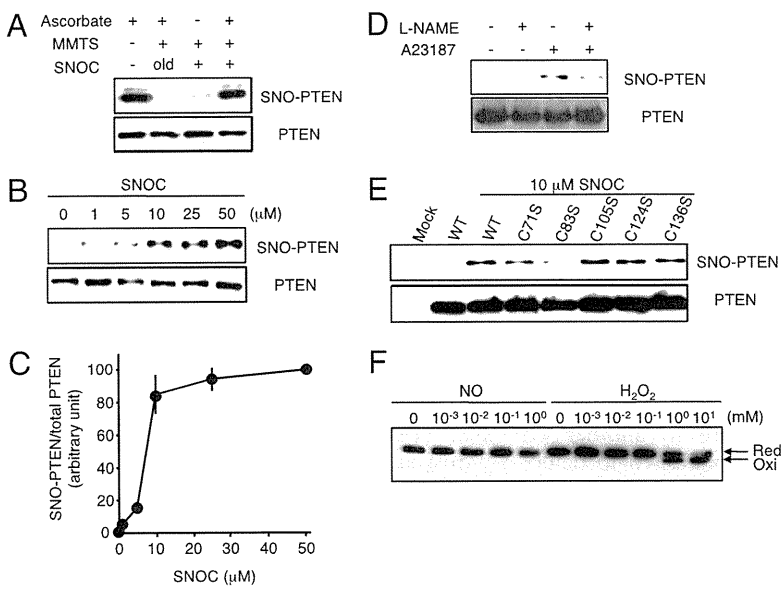

Fig. 1. *S*-nitrosylation of PTEN in vitro and in vivo. (*A, Upper*) Cell lysates from HEK293T cells were incubated with 50 μM SNOC or control solution for 20 min, followed by assay for SNO-PTEN using the biotin-switch assay. Control samples were subjected to decayed (old) SNOC. (*Lower*) Total PTEN in cell lysates was detected by Western blot. (*B, Upper*) HEK293T cells were exposed to varying concentrations of SNOC for 20 min, followed by assay for SNO-PTEN. (*Lower*) Total PTEN. (*C*) Biotin-switch assay and Western analysis were quantified by densitometry; the relative ratio of SNO-PTEN to total PTEN was calculated for each sample. Values are means ± SEM, $n = 3$. (*D, Upper*) HEK cells expressing nNOS were assayed for endogenous SNO-PTEN. nNOS was activated by Ca^{2+} ionophore A23187 (5 μM) in the presence or absence of NOS inhibitor (N^G-Nitro-L-arginine methyl ester, L-NAME, 1 mM). (*Lower*) Total PTEN. (*E, Upper*) *S*-nitrosylation of Cys-83 in PTEN. HEK cell lysates transduced with WT or C-to-S mutant FLAG-PTEN proteins were exposed to 10 μM SNOC or control for 20 min. SNO-PTEN was detected by biotin-switch assay using anti-FLAG antibody. Mutation of a critical cysteine thiol group in the phosphatase domain of PTEN(C83S) prevented *S*-nitrosylation by SNOC. (*Lower*) Total PTEN. (*F*) Effect of NO on oxidation of PTEN. HEK293 cells were incubated with the indicated concentration of SNOC or H_2O_2 for 20 min. Cell protein extracts were prepared in lysis buffer (pH 6.8) containing 40 mM *N*-ethylmaleimide and fractionated by nonreducing SDS/PAGE followed by Western analysis with anti-PTEN antibody.

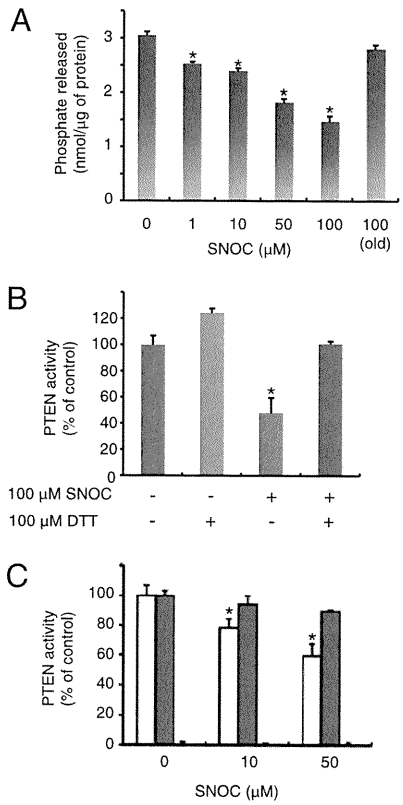

Fig. 2. *S*-nitrosylation of PTEN regulates its phosphatase activity. (*A* and *B*) Effect of *S*-nitrosylation on PTEN phosphatase activity. (*A*) In vitro expressed GST-fused PTEN was incubated with the indicated concentrations of SNOC and evaluated by phosphatase assay. (*B*) Recombinant PTEN and SNO-PTEN were assayed for lipid phosphatase activity against PI(3,4,5)P3 with or without DTT. Release of phosphate was detected colorimetrically with Biomol green reagent. Values are means ± SEM, $n = 5$; $^*P < 0.01$ by ANOVA. (*C*) GST-fused WT-PTEN (white), PTEN(C83S) (green), and dominant-negative PTEN(C124S) (black) were expressed and purified from bacteria, exposed to SNOC, and assayed for phosphatase activity. Values, expressed as percentage of WT in the absence of SNOC, are means ± SEM, $n = 5$; $^*P < 0.01$ by ANOVA.

Low Concentrations of NO Inhibit PTEN to Increase Akt Activity. Because PTEN phosphatase activity negatively regulates the PI3-kinase/Akt signaling cascade and acts upstream of Akt (17–19), we speculated that PTEN inhibition induced by *S*-nitrosylation might activate the Akt pathway. Therefore, we first investigated how various concentrations of SNOC affected Akt activity and its downstream cascade. We found that a relatively low concentration of SNOC (10 μM) markedly increased the level of phosphorylated Akt (pAkt; at Thr-308 and Ser-473) in a time-dependent fashion (Fig. 3 *A* and *B*). In contrast, high SNOC concentrations (e.g., 250 μM) did not result in increased pAkt (Fig. 3*A*), even though SNO-PTEN formation was still evident at >50 μM SNOC (Fig. 1*B*). Thus, under these conditions the increase in pAkt levels appeared only after exposure to low concentrations (10 μM) of SNOC and not after high concentrations (250 μM). We next monitored Akt activity in cells in response to various concentrations of SNOC. Low concentrations of SNOC (≤10 μM) enhanced, whereas high concentrations (≥250 μM) attenuated, substrate phosphorylation by Akt (peNOS at Ser-1177; Fig. 3 *C* and *D*).

Next, we expressed PTEN(C83S), the nonnitrosylatable mutant of PTEN, in cells to further confirm that attenuation of PTEN phosphatase activity by NO is involved in Akt activation. After transfection with PTEN(C83S), low concentrations of SNOC no longer enhanced pAkt levels, consistent with the notion that inhibition of WT PTEN enzymatic activity that we observed after *S*-nitrosylation leads to stimulation of a downstream cascade involving Akt (Fig. 3*E*). In contrast, we observed that after exposure to high concentrations of an NO donor (≥100 μM), not only PTEN but also Akt was *S*-nitrosylated, and thus Akt was directly inhibited (Fig. 3*F*), which is consistent with prior reports (24–26).

We then determined whether SNO-PTEN was formed after exposure to endogenous NO in nNOS- and eNOS-expressing cells. Treatment with A23187 to increase Ca^{2+}, and thus stimulate NOS, resulted in formation of SNO-PTEN, but not SNO-Akt, in both cell types. As a measure of NO generated, the amount of nitrite produced by nNOS or eNOS cells was approximately the same as that generated by 10–30 μM SNOC (Fig. S4). These findings showed that *S*-nitrosylation of PTEN is independent of NOS isoform and that it occurred in the presence of low (physiological) levels of NO (Fig. S4). In contrast, exposing primary cortical neurons to neurotoxic concentrations of NMDA (≥200 μM), which is known to generate high levels of NO, resulted in the formation of both SNO-PTEN and SNO-Akt (Fig. S5). From these results, we conclude that *S*-nitrosylation of PTEN occurred with physiological levels of NO derived from eNOS or nNOS, while Akt was also nitrosylated in the presence of pathological levels of NO generated by neurotoxic concentrations of NMDA. Moreover, our findings suggest that low (≤10 μM) concentrations of SNOC, although nitrosylating PTEN, could not *S*-nitrosylate Akt; this modification led to PTEN inhibition and consequently Akt phosphorylation/activation. Thus, the sensitivity of PTEN to NO was higher than that of Akt under physiological conditions in our experiments.

Formation of SNO-PTEN Results in Phosphorylation of Akt Substrates. We next asked whether activation of Akt after exposure of cells to low concentrations of SNOC led to phosphorylation of Akt substrates. Akt activity was assessed by measuring the level of phosphorylated mTOR (pmTOR; at Ser-2448), an Akt substrate (27). Levels of pmTOR were markedly increased after exposure to 10 μM SNOC, after a time course that paralleled Akt phosphorylation (Fig. 3 *G* and *H*). These functional observations were also consistent with the notion that low NO concentrations (≤10 μM) induced formation of SNO-PTEN, but not SNO-Akt, and consequently activated the Akt signaling cascade. To further substantiate our conclusion that activation of Akt after exposure to low concentrations of NO is dependent on *S*-nitrosylation and resultant inhibition of PTEN, we investigated the effect of wortmannin, a PI3-kinase inhibitor, on NO-induced Akt activation. Treatment with wortmannin resulted in significant attenuation of pAkt formation in response to low concentration of SNOC (Fig. 3*I*). This observation is consistent with the notion that NO stimulates Akt signaling through formation of SNO-PTEN with resultant inhibition of PTEN activity because this increase in pAkt would occur by means of increased PI3-kinase activity.

Additionally, it had been shown that eNOS is activated by Akt-dependent phosphorylation (28, 29). We therefore asked whether Akt activation after SNO-PTEN formation led to eNOS phosphorylation/activation in endothelial cells. We found that the level of phosphorylated eNOS (peNOS) protein rapidly increased and was sustained for up to 2 h after exposure to 10 μM SNOC in the mouse F2 endothelial cell line (Fig. 4 *A* and *B*). This SNOC-induced eNOS phosphorylation (at Ser-1177) was abrogated by Akt inhibitors (Fig. 4*C*; refs. 30 and 31). Next, we monitored eNOS activity by measuring the conversion of [^{3}H]arginine to [^{3}H]citrulline (32). We found that SNOC significantly augmented the formation of citrulline from arginine in an Akt inhibitor-sensitive manner (Fig. 4*D*). These findings are consistent with the notion that enhanced Akt activity, resulting from PTEN nitrosylation, leads to eNOS phosphorylation and activation.

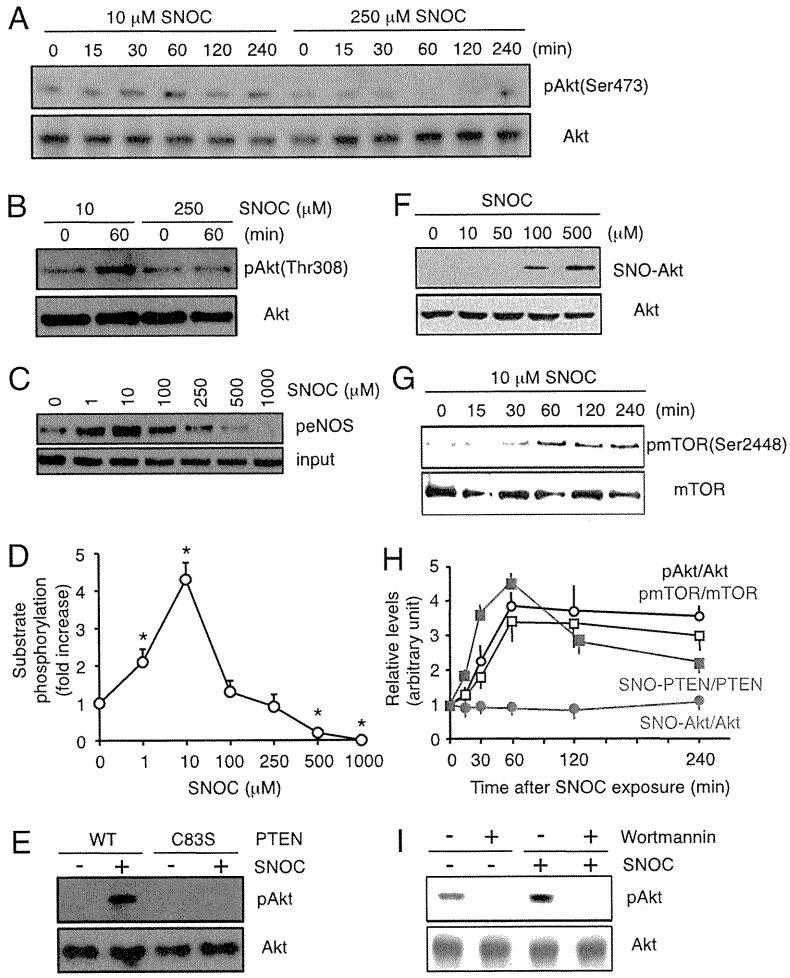

Fig. 3. *S*-nitrosylation of PTEN by low concentrations of SNOC activates the Akt pathway. (*A* and *B*) HEK293T cells were exposed to 10 or 250 μM SNOC for the indicated period. pAkt (*Upper*) and total Akt (*Lower*) were detected by Western analysis with anti-pAkt(Ser-473), anti-pAkt(Thr-308), and anti-Akt antibodies. (*C* and *D*) Akt kinase activity was enhanced by low and suppressed by high concentrations of SNOC. Kinase activity was monitored in F2 cells 30 min after exposure to SNOC by assessing phosphorylation of substrate protein eNOS using peNOS(Ser-1177) antibody. Values are means ± SEM, $n = 4$; $^*P < 0.01$ by ANOVA. (*E*) WT and PTEN(C83S) mutant-expressing HEK cells were treated with 10 μM SNOC for 1 h, and phosphorylation of Akt (Thr-308) was assessed by Western blot. (*F*) Low concentrations of SNOC did not produce SNO-Akt. (*Upper*) F2 cells were incubated with the indicated concentration of SNOC and SNO-Akt detected by biotin-switch assay. (*Lower*) Total Akt. (*G*) SNOC stimulates phosphorylation of the Akt substrate mTOR. HEK293T cells were treated with 10 μM SNOC for the indicated periods of time. pmTOR (at Ser-2448) and Akt were detected by Western analysis. (*H*) Ratio of SNO-PTEN/PTEN, SNO-Akt/Akt, pAkt/Akt, and pmTOR/mTOR levels after exposure to 10 μM SNOC. Relative intensity was quantified by using NIH Image software. Values are mean ± SEM, $n = 4$–7. (*I*) HEK293T cells were pretreated with 10 nM wortmannin for 10 min and then stimulated with 10 μM SNOC for 2 h. pAkt and total Akt were monitored as in *A*.

SNO-PTEN Inhibits Neuronal Apoptosis. To study the effect of SNO-PTEN on apoptotic cell death, we initially used an in vitro model system. For this purpose, we exposed human neural SH-SY5Y cells to staurosporine while overexpressing either WT or C83S mutant PTEN (Fig. S6). After treating the cultures with a low concentration of SNOC to activate the Akt pathway by means of SNO-PTEN formation, we found that apoptosis was significantly attenuated in WT, but not NO-insensitive C83S-PTEN mutant-expressing cells. This finding is in accord with the fact that Akt is known to be important in cell survival signaling and that it ameliorates apoptosis (33, 34).

Next, we studied the effect of SNO-PTEN formation in vivo in a rodent model of cerebral ischemia (stroke). In ischemic brain, the generation of NO contributes to neuronal cell death, and NO production is mediated, at least in part, by excessive stimulation of NMDA-type glutamate receptors (35, 36). Within 24 h of focal cerebral ischemia induced by middle cerebral artery occlusion (MCAO), cell death occurs by necrotic and apoptotic mechanisms (37). We surmised that the difference observed between the ischemic core (subcortex, including striatum) and penumbra (cortex) might be partly dependent on Akt/PTEN inactivation through *S*-nitrosylation. Although SNO-PTEN was observed in both the ischemic core and penumbral regions, SNO-Akt formation was detected only in the ischemic core and not in the penumbra (Fig. 5*A*). To compare semiquantitatively SNO-P levels in the core and penumbral regions of ischemic brains, we analyzed our blots by densitometry to calculate the ratio of SNO-PTEN or -Akt (determined by biotin-switch assay) to total PTEN or Akt (by Western blot; Fig. 5*B*). We found that the ratios of both SNO-PTEN/total PTEN and SNO-Akt/total Akt were significantly enhanced in both the ischemic core and penumbra, but only SNO-PTEN/PTEN was elevated in the penumbra. In line with these data, we also found that the levels of nitrosothiol in the core were higher than in the penumbra, as estimated by the Saville reaction on tissue samples (Fig. 5*C*). Additionally, we precipitated and then separated on SDS/PAGE biotinylated proteins (representing proteins that had been *S*-nitrosylated and subsequently labeled by the biotin-switch method) followed by silver staining to estimate the number and intensity of total SNO-Ps in the ischemic core and penumbra. The number of SNO-Ps in the ischemic core was distinctly increased compared with the penumbral region (Fig. S7). These results reveal that SNO-P formation in vivo depends upon the concentration of NO in the ischemic areas of the brains.

Our finding of enhanced levels of SNO-PTEN, but not SNO-Akt, in the penumbra led us to look for phosphorylation/activation of Akt in this region to determine whether it was indeed phosphorylated after ischemia, as would be predicted. In fact, we found that the predominant location of pAkt-positive cells was in the penumbra and not in the core. Moreover, we found that the pAkt-positive cells mostly coincided with PTEN signal in the penumbral region. In addition under our conditions, we detected fewer TUNEL-positive cells, representing apoptotic neurons, in the penumbra region than in the core region (Fig. 5 *D* and *E* and Fig. S8). These findings are consistent with the notion that in the face of low concentrations of NO in the ischemic penumbra, neuroprotection may be enhanced by Akt activation through SNO-PTEN. Hence, the ischemic model provides in vivo support

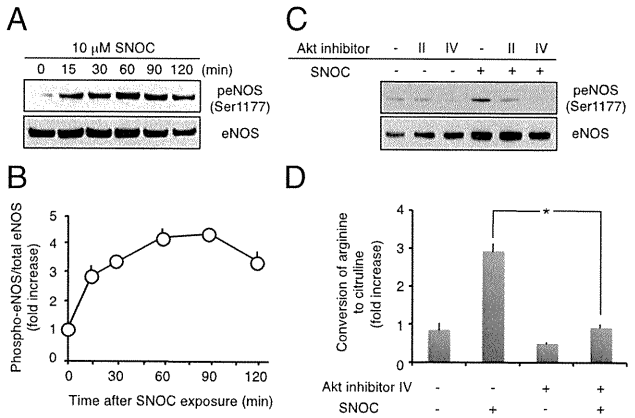

Fig. 4. *S*-nitrosylation of PTEN promotes eNOS phosphorylation by means of Akt activation. (*A*) Human endothelial F2 cells were exposed to 10 μM SNOC for the indicated periods of time. peNOS (at Ser-1177; *Upper*) and total eNOS (*Lower*) were detected by Western analysis. (*B*) Ratio of increased peNOS levels. Intensity level was quantified from blots by using NIH Image software. Values are means ± SEM, $n = 3$; $^*P < 0.01$ by ANOVA. (*C*) Akt inhibitors block phosphorylation of eNOS stimulated by exposure to SNOC. Cultures were treated with 10 μM Akt inhibitor II or IV (or control) for 30 min and then incubated with 10 μM SNOC or control solution. The levels of peNOS and eNOS were examined 30 min later by Western analysis. (*D*) eNOS activity in protein homogenates was measured with a citrulline assay. Values are means ± SEM, $n = 5$; $^*P < 0.01$ by ANOVA.

for the dependence of the positive and negative regulatory system of Akt signaling on NO concentration.

Discussion

Protein Cys thiols undergo a range of reactive nitrogen species (RNS)-dependent or reactive oxygen species (ROS)-dependent electrophilic and oxidative modifications. Through these reactions, nitrosative and oxidative stress affect the physiological function of proteins (38–41). Reversible modifications are associated with homeostatic maintenance by means of cellular redox state, but excessive amounts of RNS/ROS can elicit irreversible protein dysfunction. Here, we show that PTEN is highly sensitive to relative low concentrations of NO and that its enzymatic activity is inhibited by the resulting *S*-nitrosylation of Cys-83. In comparison, high H_2O_2 concentrations result in the oxidation of Cys residues on PTEN and formation of a disulfide bond between Cys-78 and -124. Heretofore, it has not been reported that distinct Cys residues react with NO and H_2O_2. Clues for the underlying mechanisms for these disparate reactions may lie in the 3D structure of PTEN. The atomic structure of PTEN reveals that Cys-83 is located between the pα2 and pβ4 regions (42). Asp-77, located proximal to the pα2 region, and Glu-114, located distal to the pα3 region, are both situated in the vicinity of Cys-83 in the 3D structure, showing that Cys-83 is surrounded by a motif favoring nitrosylation (43).

In the present study, we demonstrate that Cys-83 is a direct target of NO, indicating that the modification site and mode of oxidation caused by NO completely differs from H_2O_2. In contrast to Cys-83, Cys-124 is located in the enzymatic active site of PTEN and forms a disulfide bond with Cys-71 after exposure to high concentrations of H_2O_2 (22).

Because *S*-nitrosylation of PTEN inhibits its enzymatic activity, we also found that low concentrations of NO result in less dephosphorylation on Akt and thus increased Akt activity. In contrast to *S*-nitrosylation of PTEN, SNO-Akt formation results in inhibition of Akt activity (24–26). However, in the present study we show that higher concentrations of NO are necessary to *S*-nitrosylate Akt than PTEN. Thus, in the presence of low (physiological) concentrations of NO, SNO-PTEN formation would enhance Akt signaling activity, whereas high (pathological) levels of NO would *S*-nitrosylate Akt to inhibit its function directly or might act on an unknown upstream target to attenuate Akt phosphorylation. Transnitrosylation from one SNO-P to another has recently been demonstrated for several proteins (1–3, 44), so it is possible that under some circumstances SNO-Akt could transfer NO to PTEN because PTEN is a better NO acceptor than Akt. However, for the same reason, it is unlikely that the converse is true—i.e., that Akt activity is attenuated by transnitrosylation derived from SNO-PTEN at physiological concentrations of NO.

Additionally, we explored possible pathophysiological roles of *S*-nitrosylation of PTEN and Akt in vitro and in vivo. Interestingly, we found that SNO-PTEN is detected in both the core and penumbral regions of a stroke, whereas SNO-Akt is only found in the core region. Although it has been reported that PTEN can react with NO (7–13), the pathophysiological consequences of this reaction have not yet been fully elucidated. Recently, Pei et al. (11) reported that formation of SNO-PTEN occurred during brain ischemia, but the effect of *S*-nitrosylation on Akt signaling was not determined. Based on our findings, we speculate that a possible contributing factor to rescue of the penumbral region in the ischemic brain is that the lower levels

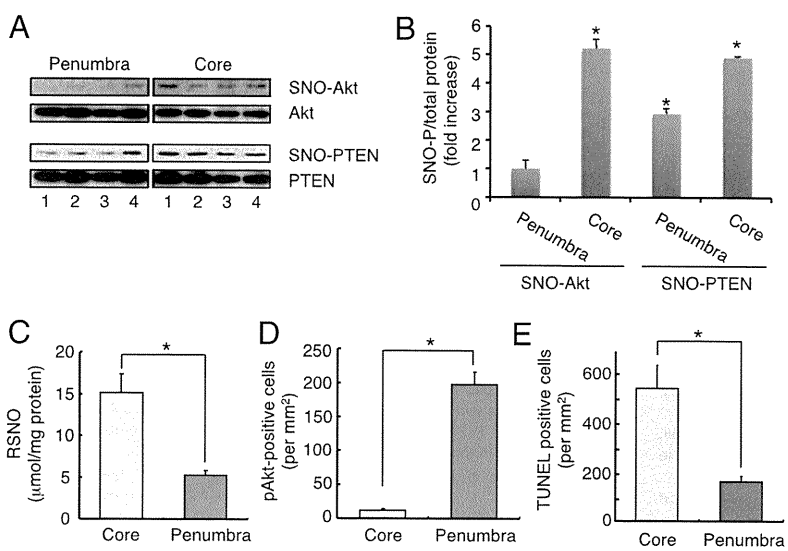

Fig. 5. *S*-nitrosylation of PTEN promotes neuroprotection through Akt activation in vitro and in vivo. (*A*) *S*-nitrosylation of PTEN and Akt after cerebral ischemia in mice. Brain tissue from infarcted hemispheres was harvested 24 h after a 2-h MCAO and subjected to biotin-switch assay to detect in vivo *S*-nitrosylation of PTEN and Akt. (*B*) Ratio of increased SNO-P to total protein. Blots from biotin-switch assays and Western analyses were quantified by densitometry, and the relative ratio of SNO-PTEN to total PTEN or SNO-Akt to total Akt in both hemispheres was calculated. Values are means ± SEM, $n = 4$; $^*P < 0.01$ by ANOVA. (*C*) NO levels, as reflected by total nitrosothiol (RSNO) in ischemic brain tissue, were measured by the Saville reaction. A significant increase in RSNO was found in both the ischemic core and penumbra. Values are means ± SEM, $n = 7$; $^*P < 0.05$ by ANOVA. (*D*) Number of pAkt-positive cells in the core and penumbra of ischemic brain. Values are means ± SEM, $n = 4$; $^*P < 0.05$ by ANOVA. (*E*) Number of TUNEL-positive apoptotic neurons in the core and penumbra of ischemic brain. Values are means ± SEM, $n = 4$; $^*P < 0.05$ by ANOVA.

of NO found in the penumbra result in *S*-nitrosylation of PTEN rather than Akt. Thus, from our findings, the penumbra, where SNO-PTEN is present in the absence of SNO-Akt, would be expected to have increased Akt neuroprotective signaling activity compared with the core of the infarct where Akt is also *S*-nitrosylated because of higher concentrations of NO.

In summary, although there have been other reports that oxidation/*S*-nitrosylation suppresses PTEN activity (22, 45), our results demonstrate the unique finding that high concentrations of NO affect not only PTEN but also downstream Akt, which thus inhibits Akt signaling and hinders cell survival in the ischemic core. Our work shows the need to characterize the sensitivity to NO of several proteins in a signaling cascade in order to determine the net effect of *S*-nitrosylation events (46).

In conclusion, our findings provide mechanistic insight into *S*-nitrosylation of PTEN, showing that PTEN is negatively regulated by lower NO concentrations than Akt and suggesting that NO could be the physiological oxidative modulator of PTEN rather than high concentrations of H_2O_2. Moreover, the fact that high concentrations of NO directly inhibit Akt activity through *S*-nitrosylation suggests the presence of a previously undescribed on–off regulatory system for Akt signaling depending on NO concentration, with low concentrations of NO activating Akt through formation of SNO-PTEN, whereas high concentrations of NO directly deactivate Akt signaling.

Materials and Methods

Materials, biotin-switch assay, screen to detect SNO-P, fluorometric detection of *S*-nitrosothiols, PTEN activity, assay for eNOS activity, PTEN oxidation, transient focal cerebral ischemia, colorimetric detection of NO_2, accumulation in brain tissue, double-immunostaining, TUNEL staining, cell counting, and cell death assay are described in *SI Materials and Methods*.

Chemicals and Antibodies. *N*-[6-(biotinamido)hexyl]-3′-(2′-pyridyldithio)propionamide was purchased from Pierce Chemical. Akt inhibitors were from Calbiochem. Anti-PTEN, anti-phospho Akt(Thr-308), anti-phospho Akt (Ser-473), anti-Akt, anti-phospho mTOR(Ser-2448), anti-mTOR, anti-phospho eNOS(Ser-1177), and anti-eNOS antibodies were obtained from Cell Signaling Technology. All other reagents were from Sigma-Aldrich.

ACKNOWLEDGMENTS. We thank Dr. Akio Matsumoto for advice; and Akane Katoh, Kana Hyakkoku, and Junya Hamanaka for excellent technical assistance. This work was supported in part by the Japan Ministry of Education, Culture, Sports and Technology (MEXT) Grants-in-Aid for Scientific Research on Innovative Areas 20117011, Scientific Research B 22310039, and Challenging Exploratory Research 21659013; the Urakami Foundation (T.U.); and National Institutes of Health Grants P01 HD29587, P01 ES016738, P30 NS057096, R01 EY09024, and R01 EY05477 (to S.A.L.).

1. Foster MW, Hess DT, Stamler JS (2009) Protein *S*-nitrosylation in health and disease: A current perspective. *Trends Mol Med* 15:391–404.
2. Liu L, et al. (2004) Essential roles of *S*-nitrosothiols in vascular homeostasis and endotoxic shock. *Cell* 116:617–628.
3. Foster MW, Forrester MT, Stamler JS (2009) A protein microarray-based analysis of *S*-nitrosylation. *Proc Natl Acad Sci USA* 106:18948–18953.
4. Doulias PT, et al. (2010) Structural profiling of endogenous *S*-nitrosocysteine residues reveals unique features that accommodate diverse mechanisms for protein *S*-nitrosylation. *Proc Natl Acad Sci USA* 107:16958–16963.
5. Jaffrey SR, Erdjument-Bromage H, Ferris CD, Tempst P, Snyder SH (2001) Protein *S*-nitrosylation: A physiological signal for neuronal nitric oxide. *Nat Cell Biol* 3:193–197.
6. Hao G, Derakhshan B, Shi L, Campagne F, Gross SS (2006) SNOSID, a proteomic method for identification of cysteine *S*-nitrosylation sites in complex protein mixtures. *Proc Natl Acad Sci USA* 103:1012–1017.
7. Yu CX, Li S, Whorton AR (2005) Redox regulation of PTEN by S-nitrosothiols. *Mol Pharmacol* 68:847–854.
8. Lim S, Clément MV (2007) Phosphorylation of the survival kinase Akt by superoxide is dependent on an ascorbate-reversible oxidation of PTEN. *Free Radic Biol Med* 42: 1178–1192.
9. Carver DJ, Gaston B, Deronde K, Palmer LA (2007) Akt-mediated activation of HIF-1 in pulmonary vascular endothelial cells by S-nitrosoglutathione. *Am J Respir Cell Mol Biol* 37:255–263.
10. Floyd RA, et al. (2007) Nitric oxide and cancer development. *J Toxicol Pathol* 20:77–92.
11. Pei DS, Sun YF, Song YJ (2009) S-nitrosylation of PTEN Invovled in ischemic brain injury in rat hippocampal CA1 region. *Neurochem Res* 34:1507–1512.
12. Sun J, Murphy E (2010) Protein S-nitrosylation and cardioprotection. *Circ Res* 106: 285–296.
13. Kwak YD, et al. (2010) NO signaling and *S*-nitrosylation regulate PTEN inhibition in neurodegeneration. *Mol Neurodegener* 5:49.
14. Mannick JB, et al. (1999) Fas-induced caspase denitrosylation. *Science* 284:651–654.
15. Ravi K, Brennan LA, Levic S, Ross PA, Black SM (2004) *S*-nitrosylation of endothelial nitric oxide synthase is associated with monomerization and decreased enzyme activity. *Proc Natl Acad Sci USA* 101:2619–2624.
16. Nott A, Watson PM, Robinson JD, Crepaldi L, Riccio A (2008) *S*-Nitrosylation of histone deacetylase 2 induces chromatin remodelling in neurons. *Nature* 455:411–415.
17. Li J, et al. (1997) PTEN, a putative protein tyrosine phosphatase gene mutated in human brain, breast, and prostate cancer. *Science* 275:1943–1947.
18. Tamura M, et al. (1998) Inhibition of cell migration, spreading, and focal adhesions by tumor suppressor PTEN. *Science* 280:1614–1617.
19. Carracedo A, Pandolfi PP (2008) The PTEN-PI3K pathway: Of feedbacks and cross-talks. *Oncogene* 27:5527–5541.
20. Maehama T, Dixon JE (1998) The tumor suppressor, PTEN/MMAC1, dephosphorylates the lipid second messenger, phosphatidylinositol 3,4,5-trisphosphate. *J Biol Chem* 273:13375–13378.
21. Stambolic V, et al. (1998) Negative regulation of PKB/Akt-dependent cell survival by the tumor suppressor PTEN. *Cell* 95:29–39.
22. Lee SR, et al. (2002) Reversible inactivation of the tumor suppressor PTEN by H_2O_2. *J Biol Chem* 277:20336–20342.
23. Okumura K, et al. (2006) PCAF modulates PTEN activity. *J Biol Chem* 281:26562–26568.
24. Yasukawa T, et al. (2005) *S*-nitrosylation-dependent inactivation of Akt/protein kinase B in insulin resistance. *J Biol Chem* 280:7511–7518.
25. Wu M, et al. (2009) Aging-associated dysfunction of Akt/protein kinase B: S-nitrosylation and acetaminophen intervention. *PLoS ONE* 4:e6430.
26. Carvalho-Filho MA, et al. (2009) Aspirin attenuates insulin resistance in muscle of diet-induced obese rats by inhibiting inducible nitric oxide synthase production and *S*-nitrosylation of IRbeta/IRS-1 and Akt. *Diabetologia* 52:2425–2434.
27. Navé BT, Ouwens M, Withers DJ, Alessi DR, Shepherd PR (1999) Mammalian target of rapamycin is a direct target for protein kinase B: Identification of a convergence point for opposing effects of insulin and amino-acid deficiency on protein translation. *Biochem J* 344:427–431.
28. Fulton D, et al. (1999) Regulation of endothelium-derived nitric oxide production by the protein kinase Akt. *Nature* 399:597–601.
29. Dimmeler S, et al. (1999) Activation of nitric oxide synthase in endothelial cells by Akt-dependent phosphorylation. *Nature* 399:601–605.
30. Kau TR, et al. (2003) A chemical genetic screen identifies inhibitors of regulated nuclear export of a Forkhead transcription factor in PTEN-deficient tumor cells. *Cancer Cell* 4:463–476.
31. Gills JJ, et al. (2007) Phosphatidylinositol ether lipid analogues that inhibit AKT also independently activate the stress kinase, p38alpha, through MKK3/6-independent and -dependent mechanisms. *J Biol Chem* 282:27020–27029.
32. Knowles RG, Palacios M, Palmer RM, Moncada S (1989) Formation of nitric oxide from L-arginine in the central nervous system: A transduction mechanism for stimulation of the soluble guanylate cyclase. *Proc Natl Acad Sci USA* 86:5159–5162.
33. Dudek H, et al. (1997) Regulation of neuronal survival by the serine-threonine protein kinase Akt. *Science* 275:661–665.
34. Kennedy SG, et al. (1997) The PI 3-kinase/Akt signaling pathway delivers an anti-apoptotic signal. *Genes Dev* 11:701–713.
35. Lei SZ, et al. (1992) Effect of nitric oxide production on the redox modulatory site of the NMDA receptor-channel complex. *Neuron* 8:1087–1099.
36. Lipton SA, Rosenberg PA (1994) Excitatory amino acids as a final common pathway for neurologic disorders. *N Engl J Med* 330:613–622.
37. Wei L, Ying DJ, Cui L, Langsdorf J, Yu SP (2004) Necrosis, apoptosis and hybrid death in the cortex and thalamus after barrel cortex ischemia in rats. *Brain Res* 1022:54–61.
38. Yao D, et al. (2004) Nitrosative stress linked to sporadic Parkinson's disease: S-nitrosylation of parkin regulates its E3 ubiquitin ligase activity. *Proc Natl Acad Sci USA* 101:10810–10814.
39. Uehara T, et al. (2006) *S*-nitrosylated protein-disulphide isomerase links protein misfolding to neurodegeneration. *Nature* 441:513–517.
40. Fang J, Nakamura T, Cho DH, Gu Z, Lipton SA (2007) *S*-nitrosylation of peroxiredoxin 2 promotes oxidative stress-induced neuronal cell death in Parkinson's disease. *Proc Natl Acad Sci USA* 104:18742–18747.
41. Cho DH, et al. (2009) *S*-nitrosylation of Drp1 mediates β-amyloid-related mitochondrial fission and neuronal injury. *Science* 324:102–105.
42. Lee JO, et al. (1999) Crystal structure of the PTEN tumor suppressor: Implications for its phosphoinositide phosphatase activity and membrane association. *Cell* 99: 323–334.
43. Stamler JS, Toone EJ, Lipton SA, Sucher NJ (1997) (S)NO signals: Translocation, regulation, and a consensus motif. *Neuron* 18:691–696.
44. Nakamura T, et al. (2010) Transnitrosylation of XIAP regulates caspase-dependent neuronal cell death. *Mol Cell* 39:184–195.
45. Delgado-Esteban M, Martin-Zanca D, Andres-Martin L, Almeida A, Bolaños JP (2007) Inhibition of PTEN by peroxynitrite activates the phosphoinositide-3-kinase/Akt neuroprotective signaling pathway. *J Neurochem* 102:194–205.
46. Lipton SA, et al. (1993) A redox-based mechanism for the neuroprotective and neurodestructive effects of nitric oxide and related nitroso-compounds. *Nature* 364: 626–632.

J Pharmacol Sci 117, 295 – 306 (2011)

Journal of Pharmacological Sciences

Full Paper

Function and Regulation of Endothelin Type A Receptor–Operated Transient Receptor Potential Canonical Channels

Takahiro Horinouchi[1], Koji Terada[1], Tsunaki Higa[1], Hiroyuki Aoyagi[1], Tadashi Nishiya[1], Hiroyuki Suzuki[1], and Soichi Miwa[1,*]

[1]*Department of Cellular Pharmacology, Hokkaido University Graduate School of Medicine, Hokkaido 060-8638, Japan*

Received September 7, 2011; Accepted October 26, 2011

Abstract. The purpose of this study is to identify transient receptor potential canonical (TRPC) channels responsible for receptor-operated Ca^{2+} entry (ROCE) triggered by activation of endothelin type A receptor (ET_AR) and to clarify the importance of calmodulin (CaM) / inositol 1,4,5-trisphosphate (IP_3) receptor binding (CIRB) domain at the C terminus of TRPC channels in ET_AR-activated channel regulation. In HEK293 cells coexpressing ET_AR and one of seven TRPC isoforms, ET_AR stimulation induced ROCE through TRPC3, TRPC5, TRPC6, and TRPC7. The TRPC3- and TRPC6-mediated ROCE was inhibited by selective inhibitors of G_q protein, phospholipase C (PLC), and CaM. The CIRB domain deletion mutants of TRPC3 and TRPC6 failed to induce ET_AR-mediated ROCE. Either deletion of the CIRB domain or pharmacological inhibition of CaM did not inhibit the targeting of these channels to the plasma membrane. These results suggest that 1) TRPC3, TRPC5, TRPC6, and TRPC7 can function as ET_AR-operated Ca^{2+} channels; 2) G_q protein, PLC, and CaM are involved in TRPC3- and TRPC6-mediated ROCE; 3) ET_AR-mediated activation of TRPC3 and TRPC6 requires the CIRB domain; and 4) abolition of ET_AR-induced ROCE by CIRB domain deletion and CaM inhibition is due to loss of CaM binding to the channels but not loss of cell surface TRPC3 and TRPC6.
[Supplementary Figures: available only at http://dx.doi.org/10.1254/jphs.11162FP]

Keywords: endothelin type A receptor, receptor-operated Ca^{2+} influx, transient receptor potential canonical (TRPC) channel, calmodulin, CaM/IP_3 receptor binding domain (CIRB)

Introduction

Endothelin type A receptor (ET_AR) is one of the G_q protein–coupled receptors (G_qPCRs) linked to phospholipase C (PLC) that hydrolyzes a phosphoinositide, phosphatidylinositol bisphosphate (PIP_2), in the plasma membrane to form two potent second messengers, cytosolic inositol 1,4,5-trisphosphate (IP_3) and membrane-bound diacylglycerol (DAG) (1 – 3). In general, a rise in the production of IP_3 and DAG after stimulation of ET_AR with its agonist endothelin-1 (ET-1) results in a transient increase and a subsequent sustained increase in intracellular free Ca^{2+} concentration ($[Ca^{2+}]_i$) (4). The binding of IP_3 to its receptors on the endoplasmic reticulum (ER) triggers Ca^{2+} release from the ER, followed by slowly developing store-operated Ca^{2+} entry (SOCE) through store-operated Ca^{2+} channels (SOCCs) (5). On the other hand, DAG can activate directly or indirectly receptor-operated Ca^{2+} channels (ROCCs) that induce receptor-operated Ca^{2+} entry (ROCE) (6). Our previous studies using whole-cell patch clamp and $[Ca^{2+}]_i$ measurement have shown that stimulation of endogenous ET_AR in vascular smooth muscle cells and of human recombinant ET_AR expressed in Chinese hamster ovary cells induces ROCE via nonselective cation channels (NSCCs) that are activated independently of store depletion (1, 7 – 9). However, the molecular entity of ET_AR-activated ROCC is not fully elucidated.

Transient receptor potential canonical (TRPC) channels have been identified as potential candidates for SOCCs and ROCCs (receptor-activated NSCCs), and they are operated by the emptying of the intracellular

*Corresponding author. smiwa@med.hokudai.ac.jp
Published online in J-STAGE on December 1, 2011 (in advance)
doi: 10.1254/jphs.11162FP

Ca^{2+} store and/or PLC-mediated DAG production following stimulation of G_qPCRs. The TRPC family consisting of TRPC1–7 is divided phylogenetically into four distinct subfamilies (TRPC1; TRPC2; TRPC3, 6, and 7; TRPC4 and 5) (10). Although the downstream molecule of the G_q protein/PLC pathway responsible for activating the receptor-operated TRPC channels is still controversial, it is well established that exogenous application of DAG directly activates TRPC3 and its close relatives, TRPC6 and TRPC7, independently of IP_3 action or store depletion (6, 11). Consequently, DAG-sensitive TRPC3, TRPC6, and TRPC7 are predicted to function as G_qPCR-activated ROCCs rather than SOCCs. TRPC4 and TRPC5 are also reported to form NSCCs that integrate signaling pathways from G_q protein–coupled muscarinic receptors and some types of receptor tyrosine kinases independently of store depletion, indicating their nature as ROCCs (12). However, it is still unknown which TRPC channels form ET_AR-operated Ca^{2+} channels that can function independently of store depletion.

Increasing evidence demonstrates that the calmodulin (CaM) / inositol 1,4,5-trisphosphate (IP_3) receptor binding (CIRB) domain conserved in the C terminus of all mammalian TRPC channels is involved in the regulation of TRPC channel function (13, 14), but its effects on the channel activity appear to vary among different TRPC isoforms. Previous studies have reported that the association of Ca^{2+}-activated CaM to the CIRB domain of TRPC channels attenuates the interaction of TRPC channels with IP_3R, resulting in loss of activation of TRPC1 (15), TRPC3 (16), TRPC4 (17), and TRPC6 (18), while the association induces activation of TRPC5 (19), TRPC6 (14), and TRPC7 (19). These studies were mainly based on functional studies such as $[Ca^{2+}]_i$ measurement and patch clamp studies with inside-out patches. Therefore, it has been unknown whether the functional changes of TRPC channels by CaM binding to the CIRB domain are accompanied by changes in the subcellular localization such as translocation of TRPC channels from the intracellular compartments to the plasma membrane.

Wedel et al. (13) have simultaneously examined changes in the subcellular localization of TRPC3 and in the ROCE following the deletion of CIRB domain in TRPC3. This study has implicated an important role of the CIRB domain in the targeting of TRPC3 to the plasma membrane, based on the finding that the deletion of the CIRB domain in TRPC3 induces loss of ROCE and translocation of the channel from the plasma membrane to intracellular compartments. The conclusion about the subcellular localization of TRPC3 in this study is based mainly on confocal microscopic imaging. However, it is well-known that quantitative assessment of target proteins localized to the cell surface by confocal microscopic imaging is not necessarily accurate. Thus, it remains to be determined whether the CIRB domain is involved in the subcellular distribution of TRPC channels.

In the present study, we first tried to elucidate TRPC channels functioning as ET_AR-operated Ca^{2+} channels and subsequently, the regulatory mechanism of the channels, focusing on the role of CIRB domain of TRPC channels in the regulation of channel function by itself and of targeting of the channels to the plasma membrane. To obtain quantitative data regarding targeting of the channels to the plasma membrane, we used a biotinylation assay in addition to confocal microscopic imaging.

We have identified ET_AR-operated TRPC channels including TRPC3 and TRPC6. The ET_AR-mediated ROCE via TRPC3 and TRPC6 was dependent on G_q protein, PLC, and CaM. In contrast to previous results from confocal microscopic imaging (13), we have demonstrate that the deletion of the CIRB domain in TRPC3 and TRPC6 results in abolition of ET_AR-induced ROCE without loss of cell surface TRPC3 and TRPC6.

Materials and Methods

Materials

YM-254890 was kindly provided by Astellas Pharma, Inc. (Tokyo). The following drugs and reagents were used in the present study: synthetic human ET-1 (Peptide Institute, Osaka); fura-2/acetoxymethyl ester (fura-2/AM) and Pluronic F-127 (Dojindo Laboratories, Kumamoto); gadolinium (III) chloride, G418, thapsigargin (TG), probenecid, puromycin dihydrochloride, aprotinin, leupeptin, pepstatin, sodium deoxycholate, sodium dodecyl sulfate (SDS), phenylmethylsulfonyl fluoride (PMSF), Na_3VO_4, NaF, and bovine serum albumin (BSA) (Sigma-Aldrich Co., St. Louis, MO, USA); U-73122 {1-[6-((17β-3-methoxyestra-1,3,5(10)-trien-17-yl)amino)hexyl]-1*H*-pyrrole-2,5-dione}, W-13 hydrochloride [*N*-(4-aminobutyl)-5-chloro-2-naphthalenesulfonamide, HCl], 1-oleoyl-2-acetyl-*sn*-glycerol (OAG) (Calbiochem, San Diego, CA, USA). Dulbecco's modified Eagle's medium (D-MEM), penicillin–streptomycin solution, and fetal calf serum (FCS) were obtained from Wako Pure Chemical Industries, Ltd. (Osaka), Sigma-Aldrich Co., and Invitrogen Corp. (Grand Island, NY, USA), respectively. Monoclonal antibody for green fluorescent protein (GFP) was obtained from Clontech Laboratories, Inc. (Mountain View, CA, USA). Monoclonal antibodies for β-actin and glyceraldehyde-3-phosphate dehydrogenase (GAPDH) were obtained from Santa Cruz Biotechnology, Inc. (Santa Cruz, CA, USA).

Construction of retrovirus vectors

The pCI-neo mammalian expression vectors encoding TRPC1 to TRPC7 were generously provided by Dr. Yasuo Mori (Kyoto University, Kyoto). The insert cDNAs of wild-type TRPC1 to TRPC7 were generated from these vectors as templates by a PCR reaction with specific primers containing the restriction enzyme sites for subcloning into the pCR™-Blunt II-TOPO™ vector (Invitrogen Corp.). The resulting pCR™-Blunt II-TOPO™ vectors and the pEGFP-N1 vector encoding a red-shifted variant of GFP (Clontech Laboratories, Inc.) were digested with two restriction enzymes simultaneously. The cDNA fragments were ligated into the pMXrmv5 retrovirus vector to yield the pMXrmv5 vectors encoding GFP and TRPC tagged with GFP at the C terminus (TRPC1-GFP, TRPC3-GFP, TRPC4-GFP, TRPC5-GFP, TRPC6-GFP, and TRPC7-GFP). The CIRB domain at the C terminus of TRPC3-GFP and TRPC6-GFP were deleted by using the KOD-Plus-Mutagenesis Kit (TOYOBO Co., Ltd., Osaka) to generate TRPC3(Δ749-783)-GFP and TRPC6(Δ840-874)-GFP. All of the constructs were verified by DNA sequencing.

Cell culture

Human embryonic kidney 293 (HEK293) cells were grown in D-MEM supplemented with 10% (v/v) FCS, penicillin (100 units·ml^{-1}), and streptomycin (100 μg·ml^{-1}) at 37°C in humidified air with 5% CO_2.

Stable expression of human ET_AR in HEK293 cells

The pDisplay mammalian expression vector containing cDNA of human ET_AR fused with an influenza hemagglutinin (HA) epitope tag at the N terminus (HA-ET_AR) was transfected into HEK293 cells by using the TransIT™-293 transfection kit (Mirus Bio Corporation, Madison, WI, USA) according to the manufacturer's instructions. Stable transformants were selected in medium containing 800 μg·ml^{-1} G418 for 3 weeks. Clonal cell lines were obtained by limiting dilution. Clones were expanded and screened for expression levels by western blot analysis. The resulting suitable clone was grown up for further experiments.

Stable expression of TRPC3, TRPC6, and their mutants

To generate HEK293 cells stably expressing one of the following proteins: GFP, TRPC1-GFP, TRPC3-GFP TRPC4-GFP, TRPC5-GFP, TRPC6-GFP, TRPC7-GFP, and GFP-tagged TRPC mutants, these genes were introduced into HEK293 cells stably expressing HA-ET_AR by retroviral gene transfer. Briefly, retroviruses were produced by triple transfection of HEK293T cells with retroviral constructs along with gag-pol and vesicular stomatitis virus G glycoprotein expression constructs (20). The supernatants containing virus were collected 24 h after transfection and added to HEK293 cells stably expressing HA-ET_AR. The HEK293 cells were then centrifuged at 900 × *g* for 45 min at 25°C followed by incubation for 6 h at 37°C in 5% CO_2 95% air. Then, fresh culture medium was added to dilute supernatants containing virus. GFP- or TRPC-GFP–positive cells were selected for growth in medium containing 5 μg·ml^{-1} puromycin for a week.

Measurement of intracellular free Ca^{2+} concentration ($[Ca^{2+}]_i$)

$[Ca^{2+}]_i$ was monitored by using a fluorescent Ca^{2+} indicator, fura-2/AM, as described previously (21 – 23). Briefly, HEK293 cells grown in a 3.5-cm dish were incubated with 4 μM fura-2/AM admixed with 2.5 mM probenecid and 0.04% Pluronic F-127 at 37°C for 45 min under reduced light. After collecting and washing cells, the cells were suspended in Ca^{2+}-free Krebs-HEPES solution (140 mM NaCl, 3 mM KCl, 1 mM $MgCl_2 \cdot 6H_2O$, 11 mM D-(+)-glucose, 10 mM HEPES; adjusted to pH 7.3 with NaOH) at 4 × 10^5 cells·ml^{-1}. $CaCl_2$ was added to a 0.5-ml aliquot of the cell suspension at the final concentration of 2 mM, when necessary. Changes of $[Ca^{2+}]_i$ in cells were measured at 30°C using a CAF-110 spectrophotometer (JASCO, Tokyo) with the excitation wavelengths of 340 and 380 nm and emission wavelength of 500 nm (bandwidth ± 10 nm).

Confocal microscopy

Confocal microscopic images were collected by using FluoView™ FV300 (Olympus Corporation, Tokyo) with a 63 × oil-immersion lens.

Biotinylation of cell surface TRPC proteins

HEK293 cells stably coexpressing HA-ET_AR and one of TRPC proteins [TRPC3-GFP, TRPC6-GFP, TRPC3(Δ749-783)-GFP, or TRPC6(Δ840-874)-GFP] grown in a 3.5-cm dish were washed twice with Ca^{2+}-free Krebs-HEPES solution. The cells were treated with drugs as indicated in Fig. 7, when necessary. The reactions were stopped 12 min after the last addition of drug by aspiration of the solution and by quick cooling on an ice/water bath. The cells were washed three times with ice-cold PBS (pH 7.4) and labeled with biotin [0.6 mg EZ-Link™ Sulfo-NHS-SS-Biotin (Thermo Fisher Scientific, Inc., Rockford, IL, USA) in 0.6 ml of PBS for each sample] at 4°C for 1 h. The reactions were quenched by adding 0.4 ml of 50 mM Tris-HCl (pH 8.0) in PBS. The cells were washed twice with ice-cold PBS and lysed with 0.35 ml RIPA buffer [150 mM NaCl, 1.5 mM $MgCl_2$, 50 mM Tris-HCl (pH 6.8), 1% NP-40, 0.5 % sodium deoxycholate, 0.1% SDS, 1 mM PMSF, 1 mM

Na_3VO_4, 20 mM NaF, 10 $\mu g \cdot ml^{-1}$ leupeptin, 10 $\mu g \cdot ml^{-1}$ aprotinin, and 10 $\mu g \cdot ml^{-1}$ pepstatin] supplemented with EDTA-free, protease inhibitor cocktail (Thermo Fisher Scientific, Inc.). The cell lysates were sonicated for 10 s on setting 10 of a handy sonicator (UR-20P; TOMY SEIKO Co., Ltd., Tokyo) and centrifuged at 20,000 × *g* for 20 min at 4°C. Protein content of the supernatant was measured according to the method of Bradford (24) using BSA as a standard.

To assay for biotinylated TRPC proteins, the lysates were incubated with 25 μl of NeutrAvidin agarose beads (Thermo Fisher Scientific, Inc.) at 4°C for 1 h. The precipitates were washed three times with the washing buffer [150 mM NaCl, 1.5 mM $MgCl_2$, 50 mM Tris-HCl (pH 6.8), 1% NP-40, 0.5% sodium deoxycholate, 0.1% SDS] and the biotinylated proteins bound to the beads were eluted by adding 50 μl of SDS sample buffer [62.5 mM Tris-HCl (pH 6.8), 10% glycerol, 5% 2-mercaptoethanol (2-ME), 2.5% SDS, 0.1% bromphenol blue] followed by incubation at 37°C for 30 min. The resulting supernatant containing biotinylated proteins was subjected to western blotting analysis to determine plasma membrane TRPC proteins. The supernatant was also analyzed for the presence of β-actin and GAPDH to determine whether cytosolic proteins were also biotinylated by our procedure. Although both β-actin and GAPDH can be easily detected in the whole cell lysates, these proteins were not biotinylated (data not shown), indicating no biotinylation of cytoplasmic proteins.

Western blot analysis

The proteins in precipitates and whole cell lysates were separated on a 5% – 20% polyacrylamide gel (SuperSep™; Wako Pure Chemical Industries, Ltd.) and electrotransferred to a polyvinylidene fluoride membrane (Immobilon™-P, pore size 0.45 μm; Millipore Corp., Bedford, MA, USA) with a semidry electroblotter. After transfer, the membranes were washed three times for 5 min with Tris-buffered saline–Tween 20 [TBS-T; 10 mM Tris-HCl (pH 8.0), 100 mM NaCl, and 0.1% Tween 20] followed by blocking (2% non-fat dry milk in TBS-T) of nonspecific binding for 1 h at room temperature. The membranes were incubated with a monoclonal antibody for GFP, β-actin, or GAPDH as a primary antibody overnight at 4°C. The primary antibody was detected with a secondary horseradish peroxidase–conjugated anti-mouse IgG antibody and enhanced chemiluminescence (ECL; GE Healthcare UK, Ltd., Little Chalfont, Buckinghamshire, UK) or ImmunoStar™ LD (Wako Pure Chemical Industries, Ltd.). The blots were exposed to Amersham Hyperfilm™ ECL (GE Healthcare UK, Ltd.). The amounts of biotinylated TRPC proteins were analyzed with National Institutes of Health ImageJ 1.37 software.

Data analysis

Data regarding change in $[Ca^{2+}]_i$ were collected and analyzed by using a MacLab/8s with Chart (v. 3.5) software (ADInstruments Japan, Tokyo). The concentration–response curves for ET-1 were constructed to evaluate its EC_{50} value, which is the effective ET-1 concentration (M) eliciting a half-maximal response, using GraphPad PRISM™ (version 3.00; GraphPad Software Inc., San Diego, CA, USA). The EC_{50} values were converted to negative logarithmic values (pEC_{50}) for analysis. All data are presented as the mean ± S.E.M. where n refers to the number of experiments. The significance of the difference between mean values was evaluated with GraphPad PRISM™ by Student's paired or unpaired *t*-test. A *P*-value less than 0.05 was considered to indicate significant differences.

Results

Identification of TRPC isoforms functioning as ET_AR-operated Ca^{2+} channels

To identify TRPC isoforms functioning as ET_AR-activated Ca^{2+} channels, HEK293 cells stably coxpressing HA-ET_AR and GFP or one of the TRPC channels tagged with GFP at the C terminus were generated as indicated in "Materials and Methods". To distinguish between SOCE and ROCE, we employed the TG-induced Ca^{2+}-depletion/Ca^{2+}-restoration protocol to measure SOCE followed by ET_AR stimulation to measure ROCE (25). Extracellular medium containing 10 μM Gd^{3+} was used throughout the experiments to inhibit the endogenous capacitative Ca^{2+} entry (SOCE) that masks the ROCE via TRPC3 and TRPC7 in HEK293 cells (19). As shown in Fig. 1, in nominally Ca^{2+}-free solution, 2 μM TG evoked Ca^{2+} mobilization from the ER, causing a transient increase in $[Ca^{2+}]_i$ that promptly returned to near baseline. In the TG-treated HEK293 cells expressing GFP as a control, addition of 10 nM ET-1 after restoration of extracellular Ca^{2+} to 2 mM did not produce further increase in $[Ca^{2+}]_i$ (Fig. 1A), indicating that ET_AR stimulation fails to elicit either Ca^{2+} release from the Ca^{2+} store, SOCE, or ROCE in cells not transfected with TRPC channel. Similar results were obtained in the TG-treated cells stably expressing TRPC1-GFP (Fig. 1B) and TRPC4-GFP (Fig. 1D). On the other hand, stimulation of ET_AR with 10 nM ET-1 elicited Gd^{3+}-insensitive ROCE in the TG-treated cells expressing TRPC3-GFP (Fig. 1C), TRPC5-GFP (Fig. 1E), TRPC6-GFP (Fig. 1F), and TRPC7-GFP (Fig. 1G) in a different manner. The ROCE via TRPC3-GFP consists of a transient peak (145.1 ± 13.6 nM, n = 5) and a subsequent sustained increase (47.2 ±

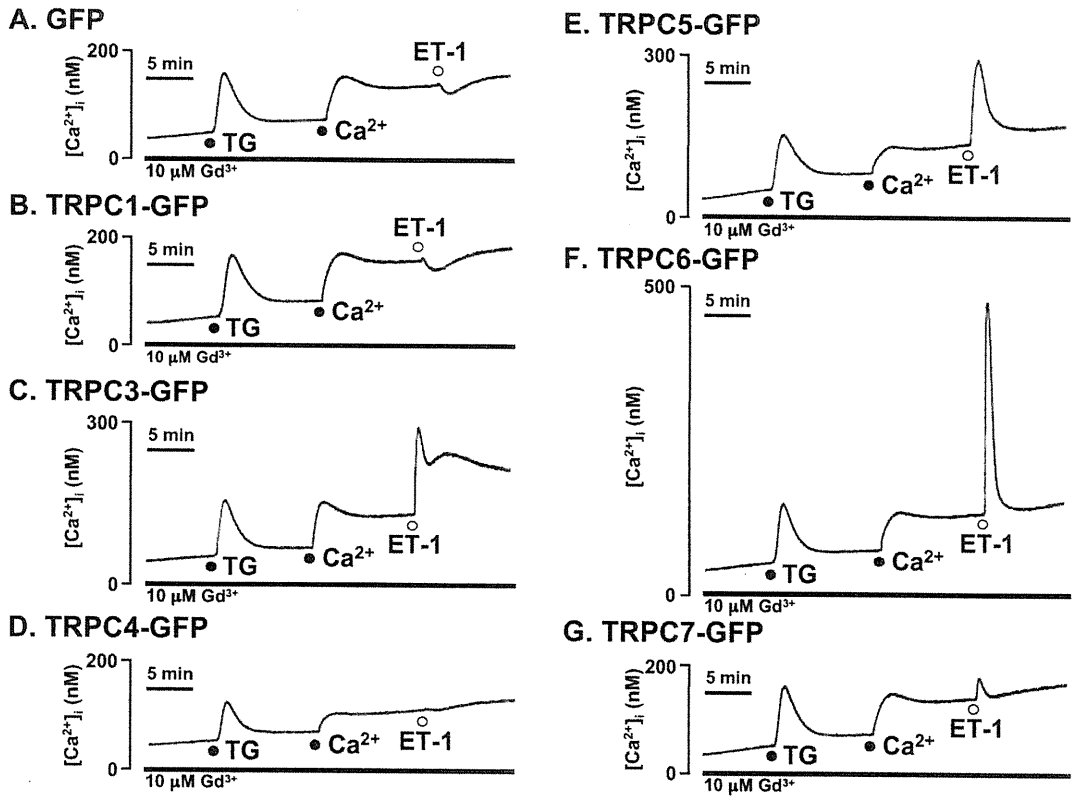

Fig. 1. Representative traces for thapsigargin (TG)-induced SOCE and ET_AR-activated ROCE after store depletion in the presence of 10 μM Gd^{3+} in GFP- (A), TRPC1- (B), TRPC3- (C), TRPC4- (D), TRPC5- (E), TRPC6- (F), and TRPC7- (G) transfected HEK293 cells stably expressing human ET_AR. TG (2 μM)-induced Ca^{2+} release from ER in nominally Ca^{2+}-free medium followed by SOCE upon restoration of 2 mM extracellular Ca^{2+}. ROCE was triggered by stimulation of ET_AR with 10 nM endothelin-1 (ET-1) 12 min after the addition of extracellular Ca^{2+}.

5.2 nM, n = 5), while the transient influx via TRPC6-GFP (324.7 ± 29.2 nM, n = 5) and TRPC7-GFP (36.2 ± 3.4 nM, n = 5) was not accompanied by a sustained phase. Unlike TRPC6-GFP and TRPC7-GFP, ROCE via TRPC5-GFP was composed of a transient phase and a weak but significant sustained phase (155.2 ± 17.2 nM for the initial phase and 31.7 ± 1.0 nM for the sustained phase, n = 5). These results suggest that TRPC3-GFP, TRPC5-GFP, TRPC6-GFP, and TRPC7-GFP are involved in ROCE induced by stimulation of ET_AR. In the present study, we focused on TRPC3- and TRPC6-mediated ROCE, since these channels are known to play an important role in onset and development of idiopathic pulmonary arterial hypertension (IPAH) that is associated with an increase in endogenous ET-1 and/or its receptor (26, 27).

Figure 2 summarizes the concentration–response curves for transient and sustained Ca^{2+} influx via TRPC3-GFP and transient Ca^{2+} entry via TRPC6-GFP. The estimated pEC_{50} values for ET-1–induced transient and sustained increase in $[Ca^{2+}]_i$ via TRPC3-GFP were 9.75 ± 0.15 and 9.42 ± 0.17 (n = 4), respectively, and the value for transient Ca^{2+} influx via TRPC6-GFP was 9.14 ± 0.06 (n = 4). To determine molecular mechanisms responsible for activation of TRPC3-GFP and TRPC6-GFP, subsequent experiments focused on the responses to ET-1 at 10 nM.

As described above (Fig. 1), the TRPC3-mediated ROCE consists of a transient peak and a subsequent sustained increase, while the TRPC6-mediated transient ROCE was not accompanied by a sustained phase. This finding suggests the possibility that the sustained Ca^{2+} influx via TRPC6 does not occur, since TRPC6 is rapidly inactivated by stimulation of ET_AR. To examine this possibility, we used the ET-1–induced Ca^{2+} release from the ER/Ca^{2+}-restoration protocol. In ET_AR-transfected HEK293 cells expressing GFP, TRPC3-GFP, or TRPC6-GFP, in nominally Ca^{2+}-free solution containing 10 μM Gd^{3+}, 10 nM ET-1 induced Ca^{2+} release from the ER, resulting in a transient increase in $[Ca^{2+}]_i$ that quickly returned to near baseline. There was no significant difference in the transient increases in $[Ca^{2+}]_i$ between them (Supplementary Fig. 1A: available in the online version only). The sustained increase in $[Ca^{2+}]_i$ in TRPC3-ex-

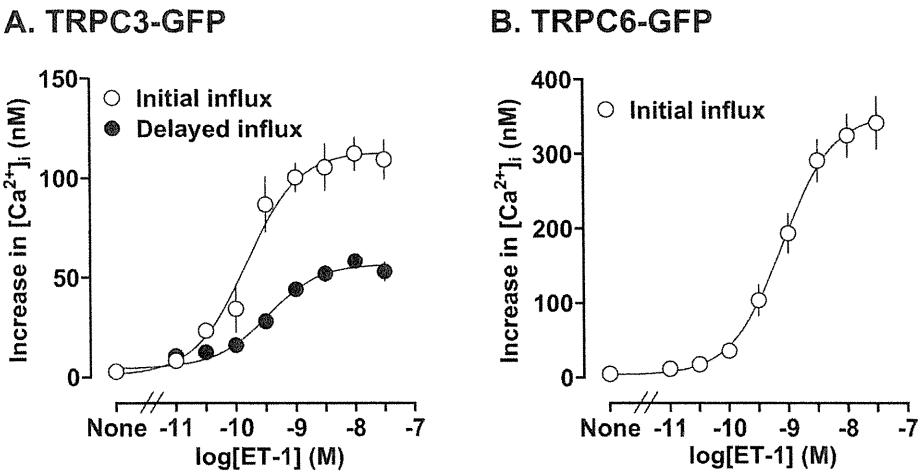

Fig. 2. Concentration response curves for ET-1 induced ROCE mediated through TRPC3 (A) and TRPC6 (B) in HEK293 cells stably coexpressing human ET_AR and TRPC3-GFP or TRPC6-GFP. Data are presented as the mean ± S.E.M. of the results obtained from 5 experiments. When no error bar is shown, the error is smaller than the symbol.

pressed cells was slightly higher than that in the cells expressing GFP or TRPC6. The restoration of extracellular Ca^{2+} to 2 mM after addition of 10 nM ET-1 evoked transient and sustained Ca^{2+} entry in these cells. Interestingly, the Ca^{2+} responses in TRPC3-expressing cells were bigger than those in GFP-expressing cells, whereas there was no significant difference in the Ca^{2+} responses between GFP-expressing and TRPC6-expressing cells (Supplementary Fig. 1B: available in the online version only). The TRPC3-mediated transient Ca^{2+} influx was insensitive to 10 μM Gd^{3+} (666.7 ± 72.4 nM in the absence of Gd^{3+} and 693.9 ± 95.8 nM in the presence of 10 μM Gd^{3+}, n = 4 for each), ruling out the involvement of SOCE. Thus, overexpression of TRPC6 had no effect on Ca^{2+} influx induced by the ET-1–induced Ca^{2+} release/Ca^{2+}-restoration protocol, in contrast to ET-1–induced, TRPC6-mediated ROCE after the TG-induced Ca^{2+}-depletion/Ca^{2+}-restoration (Fig. 1F). These results indicate that ET_AR stimulation inactivates TRPC6, leading to the failure to induce sustained Ca^{2+} entry.

Determination of signaling molecules responsible for TRPC3- and TRPC6-mediated Ca^{2+} entry in response to ET_AR stimulation by using several types of inhibitors

To determine signaling molecules regulating the TRPC3- and TRPC6-mediated Ca^{2+} entry, we examined the effects of several types of inhibitors on ROCE induced by ET_AR stimulation. As shown in Fig. 3, TRPC3- and TRPC6-mediated Ca^{2+} entry triggered by ET-1 was significantly inhibited by either 1 μM YM-254890 (a G_q protein inhibitor) (7.0% ± 1.9% of the control Ca^{2+} response for TRPC3; 1.8% ± 0.3% for TRPC6, n = 5 for each) or 3 μM U-73122 (a PLC inhibitor) (31.4% ± 7.9% for TRPC3, 32.7% ± 7.2% for TRPC6, n = 5 for each). In addition, 30 μM W-13, a CaM inhibitor, greatly reduced ET-1–induced ROCE via TRPC3 (18.9% ± 3.5%,

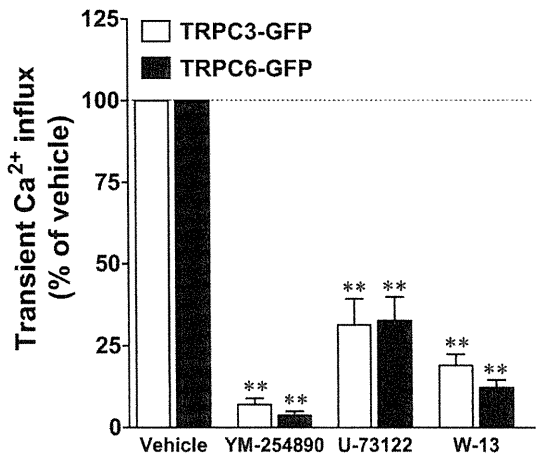

Fig. 3. Effects of YM-254890, U-73122, and W-13 on TRPC3- and TRPC6-mediated transient Ca^{2+} influx triggered by 10 nM ET-1. Data are presented as the mean ± S.E.M. of the results obtained from 4 – 6 experiments. $^{**}P < 0.01$ vs. its vehicle.

n = 4) and TRPC6 (12.3% ± 2.2%, n = 4), contrary to a previous report where CaM negatively regulated the activities of TRPC3 (16) and TRPC6 (18).

Both TRPC3 and TRPC6 are reported to be activated by elevated endogenous DAG or application of a membrane-permeable DAG analogue, OAG (11). As shown in Supplementary Fig. 2 (available in the online version only), addition of 100 μM OAG to extracellular solution induced an increase in $[Ca^{2+}]_i$ (63.2 ± 4.9 nM for TRPC3-GFP and 87.4 ± 8.5 nM for TRPC6-GFP, n = 5 for each). Although, either 1 μM YM-254890 or 3 μM U-73122 had no effect on OAG-induced Ca^{2+} influx via TRPC3 and TRPC6, the responses to OAG were inhibited by 30 μM W-13 (Supplementary Fig. 3: available in the online version only).

Importance of CIRB domain in subcellular localization and channel activity of TRPC3 and TRPC6

The CIRB domain present in the C terminus of TRPC protein (i.e., residues 749 – 783, ESHSFNSILNQPTRY QQIMKRLIKRYVLKAQVDKE for TRPC3 and 840 – 874, EDYHLNSFSNPPRQYQKIMKRLIKRYVLQAQ IDKE for TRPC6) is conserved among all TRPC homologues (17). To gain insight into the role of the CIRB domain of the TRPC3 and TRPC6 in regulating either channel activity or intracellular localization, we made GFP-tagged CIRB domain deletion mutants of TRPC3 (TRPC3(⊿749-783)-GFP) and TRPC6 (TRPC6(⊿840-874)-GFP).

To estimate the channel activity of the CIRB domain deletion mutants, we have performed a $[Ca^{2+}]_i$ measurement study. These experiments revealed that TRPC3(⊿749-783)-GFP (Fig. 4A) and TRPC6(⊿840-874)-GFP (Fig. 4B), both of which lack the CIRB domain, completely lost their ability to trigger ET_AR-operated Ca^{2+} influx, whereas wild-type TRPC3 and TRPC6 induced the ROCE upon ET_AR stimulation. Similarly, the OAG-induced Ca^{2+} entry was significantly depressed in the CIRB domain–deletion mutants of TRPC3 and TRPC6, when compared with its wild type (Supplementary Fig. 4: available in the online version only).

TRPC3 and TRPC6 expressed in HEK293T cells are reported to be present mainly on the plasma membrane (28). In our experimental systems, TRPC3-GFP (wild-type) and TRPC3(⊿749-783)-GFP were distributed diffusely throughout the cytosol as well as in punctate vesicular structures (Fig. 5A). Wild-type TRPC6-GFP was mainly targeted to the plasma membrane, whereas TRPC6(⊿840-874)-GFP was present in the cytoplasm (Fig. 5B). The fluorescence of GFP observed with confocal microscopy seems to reflect the localization of TRPC proteins but not that of GFP itself derived from the degradation of fusion proteins with GFP (29), since western blot analysis detects no signal of GFP (approximately 27 kDa) (data not shown). This is also supported by the findings that the GFP protein alone diffuses passively through the pores of the nuclear envelope due to its low molecular mass of 27 kDa and it is mainly localized in the nucleus rather than the cytoplasm and plasma membrane (30).

Plasma membrane localization of wild-type and mutant TRPC3 and TRPC6

To clarify whether the abolition of ET_AR-mediated ROCE was due to failure of mutant channels to distribute to the plasma membrane, we compared quantitatively the expression levels of these channels localized on plasma membrane by using cell surface biotinylation experiments. We first confirmed that β-actin and GAPDH, both of which are cytosolic proteins as a negative control for surface expression, were not biotinylated (data not shown), indicating that this method allows us to estimate specifically cell surface biotinylation of TRPC3 and TRPC6 proteins. We detected biotinylated TRPC3 and TRPC6 proteins in cells expressing wild-type and the CIRB domain deletion mutant (Fig. 6A). Notably, the levels for biotinylated and total proteins of mutant TRPC3 were significantly higher than the values of wild-type TRPC3: they were 336.5% ± 48.7% (n = 4) and 279.0% ± 36.2% (n = 4), respectively, of the values for wild-type (Fig. 6B). In contrast, mutant TRPC6 showed lower levels for biotinylated (70.3% ± 10.2%, n = 4) and total proteins (69.8% ± 10.4%, n = 4) compared with the wild-type (Fig. 6C). However, there was no significant difference between the ratio of mutant TRPC3 to wild-type TRPC3 for biotinylated protein and the ratio of mutant TRPC3 to wild-type TRPC3 for total protein (Fig. 6B). Similar results were obtained for wild-type and mutant TRPC6 (Fig. 6C). These results indicate that the deletion of CIRB domain does not inhibit targeting of TRPC3 and TRPC6 to cell surface.

Effects of the CaM inhibitor W-13 on the levels of cell surface TRPC3 and TRPC6

Finally, we attempted to clarify whether CaM plays an important role in the targeting of TRPC3 and TRPC6 to the plasma membrane. TG-induced Ca^{2+}-depletion/Ca^{2+}-restoration followed by ET_AR stimulation did not induce significant changes in the levels of biotinylated TRPC3 and TRPC6 (Fig. 7). In addition, pharmacological inhibition of CaM by 30 μM W-13, which suppressed the TRPC3- and TRPC6-mediated ROCE (Fig. 3), had no effect on cell surface biotinylation of TRPC3 and TRPC6. Therefore, the inhibitory effects of the CaM inhibitor W-13 on the ET_AR-mediated ROCE were not due to decreases in surface expression of TRPC3 and TRPC6.

Discussion

Extracellular Ca^{2+} influx is an important machinery to trigger various physiological and pathophysiological events such as cell proliferation, cell differentiation, neurotransmitter release, muscle contraction, apoptosis and activation of immune cells. Non-excitable cells can mainly utilize non-voltage gated, Ca^{2+}-permeable channels which are at least subdivided into two main types, either SOCC activated by the depletion of ER or ROCC activated by second messengers (e.g., DAG) generated by activation of PLC-linked G_qPCRs (31). Evidence is accumulating that all seven TRPC homologs form SOCC and/or ROCC by the homo- or hetero-multimerization of TRPC subunits in a manner similar to voltage gated K^+